Relativistic atomic data for Cu-like tungsten

U. I. Safronova, A. S. Safronova, and P. Beiersdorfer

Relativistic atomic data for Cu-like tungsten

U. I. Safronova and A. S. Safronova

Physics Department, University of Nevada, Reno, NV 89557

P. Beiersdorfer

Physics Division, Lawrence Livermore National Laboratory, Livermore, CA 94550

(Dated: October 1, 2012)

Energy levels, radiative transition probabilities, and autoionization rates for [Ne]$3s^23p^63d^94l'nl$, [Ne]$3s^23p^53d^{10}4l'nl$ (n=4-6), and [Ne]$3s^23p^63d^95l'nl$,(n=5-7) states in Cu-like tungsten (W^{45+}) are calculated using the relativistic many-body perturbation theory method (RMBPT code), the multi-configuration relativistic Hebrew University Lawrence Livermore Atomic Code (HULLAC code), and the Hartree-Fock-relativistic method (COWAN code). Autoionizing levels above the [Ne]$3s^23p^63d^{10}$ threshold are considered. It is found that configuration mixing among [Ne]$3s^23p^63d^94l'nl$ and [Ne]$3s^23p^53d^{10}4l'nl$ plays an important role for all atomic characteristics.Branching ratios relative to the first threshold and intensity factors are calculated for satellite lines, and dielectronic recombination (DR) rate coefficients are determined for the singly excited [Ne]$3s^23p^63d^{10}nl$ (n=5-7), as well as doubly excited non-autoionizing [Ne]$3s^23p^63d^94s4l$, ($l = s, p, d, f$), [Ne]$3s^23p^63d^94p4l$, ($l = p, d, f$), [Ne]$3s^23p^63d^94d^2$, [Ne]$3s^23p^53d^{10}4s4l$, ($l = s, p, d$), and [Ne]$3s^23p^53d^{10}4p^2$ states in Cu-like W^{45+} ion. Contributions from the autoionizing doubly excited states [Ne]$3s^23p^63d^94l'nl$, [Ne]$3s^23p^53d^{10}4l'nl$, and [Ne]$3s^23p^63d^95l'nl$ states (with n up to 500), which are particulary important for calculating total DR rates, are estimated. Synthetic dielectronic satellite spectra from Cu-like W are simulated in a broad spectral range from 3 to 70 Å. These calculations provide highly accurate values for a number of W^{45+} properties useful for a variety of applications including for fusion applications.

I. INTRODUCTION

Relativistic atomic data for tungsten ions and dielectronic recombination data in particular are in great demand for fusion applications. The reason is the use of tungsten as a plasma-facing component in current magnetic fusion devices as well as in the next-generation fusion reactors, notably ITER (Latin "the way"). Line emission is being studied for determining the radiative losses and power balance determinations, for assessing the ionization balance, and for developing spectroscopic diagnostics [1–9].

When discussing M-shell W ions, then Ni-like W ions and their spectra are probably the most frequently observed x-ray spectra from high-temperature laboratory plasmas from tokamak to Z-pinch and laser plasmas. The reason is that Ni-like ions have a $1s^22s^22p^63s^23p^63d^{10}$ closed-shell ground state configuration. This makes the ion very stable and exist over a broad range of plasma parameters, including the electron temperatures found in most of today's high-power plasma sources. Ni-like ions have even been used for producing x-ray lasing emission [10, 11]. Cu-like ions have one more electron than Ni-like ions, and x-ray lines from Cu-like ions are usually seen together with the Ni-like lines. The Cu-like x-ray lines can be produced by innershell excitation or by dielectronic recombination (DR). They are typically weaker than Ni-like lines for several of reasons. These include the fact that innershell-excited Cu-like levels are often autoionizing levels, which can decay without giving off an x-ray photon. Moreover, there are a large number of innershell-excited Cu-like levels within a given spectroscopic complex, compared to a rather small number of such levels in Ni-like ions. Finally, the abundance of Cu-like ions is often smaller than that of Ni-like ions at a given plasma temperature.

The atomic spectra of Cu-like W are not so well resolved and only the simplest of them are comprehensively investigated. For example, even the most well known $(3s^23p^63d^94l4l')$ configurations in Cu- like ions are of continuing interest from both theoretical and experimental points of view. Experimentally, these configurations were studied by photon and electron emission spectroscopy. To our knowledge, the first measurements of $3d − 4p$ transitions in Cu-like W and Tm were done by Klapisch *et al.* in Ref. [12] by classification of x-ray spectra from laser produced plasmas in the range 6 - 9 Å. It was shown in Ref. [12] that the most of the $3d − 4p$ Cu-like intensities come from the the the $(3s^23p^63d^{10}4s−3s^23p^63d^94s4p)$, $(3s^23p^63d^{10}4p−3s^23p^63d^94p^2)$, $(3s^23p^63d^{10}4d − 3s^23p^63d^94p4d)$, and $(3s^23p^63d^{10}4f − 3s^23p^63d^94p4f)$ transitions. The wave lengths and transition probabilities were calculated in [12] by the relativistic parametric potential (RELAC) method [13]. The same method was extended by by Mandelbaum *et al.* in Ref. [14] to study x-ray spectra from laser produced plasmas of atoms from Tm ($Z = 69$) up to Pt ($Z = 78$). The unresolved $3d − 4f$ transitions in the x-ray spectra of highly ionized Tm to Re from laser-produced plasma were studied by Klapisch *et al.* [15]. Interpretation of laser produced Au and W x-ray spectra in the 3 keV range was presented by Zigler

et al. [16]. Extended analysis of the x-ray spectra of laser-irradiated elements in the sequences from tantalum to lead was reported by Tragin *et al.* [17].

Atomic data and spectral line intensities for highly ionized tungsten (Co-like W^{47+} to Rb-like W^{37+}) in a high-temperature, low-density tokamak plasma were reported by Fournier [18]. Calculated transition wavelengths, oscillator strengths, and collisional-radiative line intensities are presented for the 11 tungsten ($Z= 74$) ions from Co-like W^{47+} to Rb-like W^{37+}. The RELAC code were carried out for the ion structure in each case.

Moreover, a spectroscopic analysis and modeling of tungsten EBIT and Z-pinch plasma experiments was presented by Osborne *et al.* in Refs. [19]. Spectroscopy of M-shell X-ray transitions in Zn-like through Co-like tungsten was investigated by Clementson *et al.* [20]. Spectra of W^{39+} - W^{47+} in the 12-20 nm region observed with an EBIT light source were investigated by Ralchenko *et al.* [21]. Wavelengths and transition probabilities for n=4→n′=4 transitions in heavy Cu-like ions ($70 \leq Z \leq$ 92 were presented by Palmeri *et al.* [22]. Fully relativistic multiconfiguration Dirac-Fock (MCDF) calculations were carried out. Theoretical results were compared with recent electron-beam ion-trap (EBIT) measurements in Cu-like ytterbium, tungsten, osmium, gold, lead, bismuth, thorium, and uranium. An overview of recent work on W ions including Cu-like W ions is given by Kramida [23].

Relativistic many-body calculations of excitation energies and transition rates from core-excited states in Cu-like ions were presented by Safronova *et al.* [24]. Energies of ($3s^23p^63d^94l4l'$), ($3s^23p^53d^{10}4l4l'$), and ($3s3p^63d^{10}4l4l'$) states for Cu-like ions with $Z = 30$–100 were evaluated to second order in relativistic many-body perturbation theory (RMBPT) starting from a Ni-like Dirac-Fock potential. Transition rates and line strengths are calculated for the $3l - 4l'$ electric-dipole (E1) transitions in Cu-like ions with nuclear charge $Z = 30$–100.

In the present paper, we evaluate energy levels, radiative transition probabilities, and autoionization rates for [Ne]$3s^23p^63d^94l'nl$, [Ne]$3s^23p^53d^{10}4l'nl$ (n=4-6), and [Ne]$3s^23p^63d^95l'nl$,(n=5-7) states in Cu-like tungsten (W^{45+}) to build synthetic spectra of Cu-like W^{45+} ion. The DR rate coefficients are determined for the singly excited [Ne]$3s^23p^63d^{10}nl$ (n=5-7), as well as for the doubly excited non-autoionizing [Ne]$3s^23p^63d^94s4l$, ($l = s,p,d,f$), [Ne]$3s^23p^63d^94p4l$, ($l = p,d,f$), [Ne]$3s^23p^63d^94d^2$, [Ne]$3s^23p^53d^{10}4s4l$, ($l = s,p,d$), and [Ne]$3s^23p^53d^{10}4p^2$ states in the Cu-like W^{45+} ion, in particular those produced by DR. Contributions from the autoionizing doubly excited states Ne]$3s^23p^63d^94l'nl$, [Ne]$3s^23p^53d^{10}4l'nl$, and [Ne]$3s^23p^63d^95l'nl$ states (with n up to 500), which are particulary important for calculating total DR rates, are estimated. Energy levels, radiative transition probabilities, and autoionization rates for those states are calculated using the COWAN, HULLAC, and RMBPT codes. These three codes allow us to check the accuracy of our calculations and to achieve

confidence that our predictions are reliable. We present the state-selective DR rate coefficients to excited states of Cu-like tungsten as well as the total DR rate coefficients as a function of electron temperature. In addition, we present a detailed comparison of our theoretical calculations with the recommended data from NIST database, which is another test the accuracy of our results. Below, we omit the core [Ne] $= 1s^22s^22p^6$ and $3s^2$ shell from the configuration notation.

II. ENERGY LEVELS, TRANSITION PROBABILITIES, AND AUTOIONIZATION RATES IN CU-LIKE TUNGSTEN

Detailed calculations of dielectronic recombination parameters should include the determination of such characteristics as energies, radiative transition probabilities, and autoionization rates for atomic states in the recombined ion. Recently, the DR parameters were evaluated in Yb-like W^{4+} [27], Er-like W^{6+} [28], Xe-like W^{20+} [29], Ag-like W^{27+} [30], and Rh-like W^{29+} [31].

We carried out detailed calculations of the radiative and autoionization rates for the intermediate states $3p^63d^94l'nl$, $3p^53d^{10}4l'nl$ (n=4-6), and $3p^63d^95l'nl$ (n=5-7) states in Cu-like tungsten. The list of the $3p^63d^{10}nl$, $3p^63d^94l'nl$, $3p^53d^{10}4l'nl$, and $3p^63d^95l'nl$ configurations consists of 80 even-parity and 74 odd-parity configurations (see Table I). The resulting list of levels included in the set of singly excited $3p^63d^{10}nl$ configurations with n=4-7 consists of 21 even-parity and 20 odd-parity states. The set of doubly excited $3p^63d^94l'nl$ and $3p^53d^{10}4l'nl$ configurations with n=4-6 consists of 4133 and 2654 levels, respectively. The set of doubly excited $3p^63d^95l'nl$ configurations with n=5-7 from Table I consists of 3101 even-parity and 1876 odd-parity states.

With almost 6 000 levels per parity, the total number of radiative transitions is in the tens of millions. To reduce the computational load, we neglected transitions with small probabilities, $A_r <10^5$ s^{-1} (the strongest transitions, as will be shown below, have A_r on the order of 10^{14} s^{-1}). Even with this restriction, the resulting list of radiative transitions within the Cu-like ion includes about 2.3×10^6 transitions.

Our large-scale calculations of atomic properties are based on the previously mentioned three atomic computer codes: the code developed by Cowan, which uses a quasi-relativistic Hartree-Fock method with superposition of configurations (in the following we will refer to it as the "COWAN" code) [32, 33], the multiconfiguration relativistic Hebrew University Lawrence Livermore Atomic Code (the HULLAC code)[34], and the Relativistic Many-Body Perturbation Theory code (the RMBPT code). The RMBPT computations were carried out with two methods, (i) the relativistic second- and third-order, and all-order RMBPT [35, 36] for the singly excited states, and (ii) the relativistic second-order for doubly excited states [37, 38].

TABLE I: Labelling of configurations for even-parity and odd-parity complexes in Cu like W^{45+}. Designations used are $3p^6 3d^{10} nl = nl$, $3p^6 3d^9 nln'l' = 3dnln'l'$, and $3p^5 3d^{10} nl = 3pnln'l'$.

| | Even-parity states | | Even-parity states | | Even-parity states | | Odd-parity states | | Odd-parity states | | Odd-parity states |
N	Configuration	N	Configuration	N	Configuration	N	Configuration	N	Configuration	N	Configuration
1	$4s$	28	$3d4p6f$	55	$3d5p7h$	1	$4p$	28	$3d4d6f$	55	$3p4s4d$
2	$4d$	29	$3d4p6h$	56	$3d5d7s$	2	$4f$	29	$3d4d6h$	56	$3p4p4f$
3	$5s$	30	$3d4d6s$	57	$3d5d7d$	3	$5p$	30	$3d5s5p$	57	$3p4s5d$
4	$5d$	31	$3d4d6d$	58	$3d5d7g$	4	$5f$	31	$3d5s5f$	58	$3p4s5g$
5	$5g$	32	$3d4d6g$	59	$3d5f7p$	5	$6p$	32	$3d5p5d$	59	$3p4p5f$
6	$6s$	33	$3d4f6p$	60	$3d5f7f$	6	$6f$	33	$3d5d5f$	60	$3p4d5s$
7	$6d$	34	$3d4f6f$	61	$3d5f7h$	7	$6f$	34	$3d5s6p$	61	$3p4d5d$
8	$6g$	35	$3d4f6h$	62	$3p4s4p$	8	$7p$	35	$3d5s6f$	62	$3p4d5g$
9	$7s$	36	$3d45s^2$	63	$3p4s4f$	9	$7f$	36	$3d5s6h$	63	$3p4f5p$
10	$7d$	37	$3d45p^2$	64	$3p4p4d$	10	$7f$	37	$3d5p6s$	64	$3p4f5f$
11	$7g$	38	$3d45d^2$	65	$3p4d4f$	11	$3d4s4p$	38	$3d5p6d$	65	$3p4s6d$
12	$3d4s^2$	39	$3d45f^2$	66	$3p4s5p$	12	$3d4s4f$	39	$3d5d6p$	66	$3p4s6g$
13	$3d4p^2$	40	$3d5s5d$	67	$3p4s5f$	13	$3d4p4d$	40	$3d5d6f$	67	$3p4p6f$
14	$3d4d^2$	41	$3d5p5f$	68	$3p4p5s$	14	$3d4d4f$	41	$3d5d6h$	68	$3p4p6h$
15	$3d4f^2$	42	$3d5s6d$	69	$3p4p5d$	15	$3d4s5p$	42	$3d5s7p$	69	$3p4d6s$
16	$3d4s4d$	43	$3d5s6g$	70	$3p4p5g$	16	$3d4s5f$	43	$3d5s7f$	70	$3p4d6d$
17	$3d4p4f$	44	$3d5p6f$	71	$3p4d5p$	17	$3d4p5s$	44	$3d5s7h$	71	$3p4d6g$
18	$3d4s5d$	45	$3d5p6h$	72	$3p4d5f$	18	$3d4p5d$	45	$3d5p7s$	72	$3p4f6p$
19	$3d4s5g$	46	$3d5d6s$	73	$3p4s6p$	19	$3d4p5g$	46	$3d5p7d$	73	$3p4f6f$
20	$3d4p5f$	47	$3d5d6d$	74	$3p4s6f$	20	$3d4d5p$	47	$3d5d7p$	74	$3p4f6h$
21	$3d4d5s$	48	$3d5d6g$	75	$3p4s6h$	21	$3d4d5f$	48	$3d5d7f$		
22	$3d4d5d$	49	$3d5f6p$	76	$3p4p6s$	22	$3d4s6p$	49	$3d5d7h$		
23	$3d4d5g$	50	$3d5f6f$	77	$3p4p6d$	23	$3d4s6f$	50	$3p4s^2$		
24	$3d4f5p$	51	$3d5f6h$	78	$3p4d6p$	24	$3d4s6h$	51	$3p4p^2$		
25	$3d4f5f$	52	$3d5s7d$	79	$3p4d6f$	25	$3d4p6s$	52	$3p4d^2$		
26	$3d4s6d$	53	$3d5s7g$	80	$3p4d6h$	26	$3d4p6d$	53	$3p4f^2$		
27	$3d4s6g$	54	$3d5p7f$			27	$3d4d6p$	54	$3p4s4d$		

The results of energy calculations for the singly excited $3p^6 3d^{10} nl$ states of W^{45+} are summarized in Table II, which presents the lowest-order Dirac-Fock (DF) energies E^{DF}, the second-order ($E^{\mathrm{DF}+2}$) and third-order Coulomb correlation energies ($E^{\mathrm{DF}+2+3}$), the all-order "SD" energies $E^{\mathrm{DF}+\mathrm{SD}}$, as well as the COWAN code results, $E^{(\mathrm{COWAN})}$. The difference between $E^{(\mathrm{COWAN})}$ values and NIST values [25] is less than 0.06% for the $6f\ ^2F_J$ and $6g\ ^2G_J$ levels, ess than 0.14% for the $5l[\ ^2S_{1/2},\ ^2P_J,\ ^2D_J,\ ^2F_J,\ ^2G_J]$ levels. The largest difference (1.8%) between $E^{(\mathrm{COWAN})}$ values and NIST values [25] is for the $4p\ ^2P_{1/2}$ level, while the difference for the $4p\ ^2P_{3/2}$ and $4d\ ^2D_J$ levels is equal to 0.9% and 0.3%, respectively. The second-order correlation contributions to the E^{DF} values are the largest one (0.3% - 0.6%) for the $4l[\ ^2S_{1/2},\ ^2P_J,\ ^2D_J,\ ^2F_J]$ levels and about 0.1% - 0.15% for other levels. There is a very small contribution of the third-order contribution; the difference in results given in columns $E^{\mathrm{DF}+2+3}$ and $E^{\mathrm{DF}+2}$ of Table II is less than 0.01%. Our third-order Coulomb correla-

tion energies ($E^{\mathrm{DF}+2+3}$) and the all-order "SD" energies $E^{\mathrm{DF}+\mathrm{SD}}$ are in excellent agreement (0.002-0.1%) with the recommended NIST data [25]. Such good agreement with the available NIST energies allows us to believe that our $E^{\mathrm{DF}+\mathrm{SD}}$ energies for the $6s\ ^2S_{1/2}$, $6p\ ^2P_J$, and $6d\ ^2D_J$ levels given in Table II should be used as recommended data. The last line of Table II presents the RMBPT value for the ionization potential of W^{45+}. We also find excellent agreement (0.033%) between our "SD" I.P. values and the recommended NIST I.P. values [25].

In Table III, we present wavelengths, weighted oscillator strengths, and weighted radiative transition rates gA_r for the $3p^6 3d^{10} n_1 l_1 - 3p^6 3d^{10} n_2 l_2$ transitions of Cu-like tungsten. Results for the oscillator strengths and transition rates are presented in the DF lowest-order RMBPT approximation (columns 6 and 9 of Table III) and the all-order RMBPT approximation (columns "DF+SD"). It should be noted that these lowest order RMBPT values agree with the results evaluated in the MCDF approach. To obtain the all-order matrix elements, we first

TABLE II: Energies (E in 10^3 cm^{-1}) calculated to the first-, second-, third-, and all-orders of RMBPT for the $3p^63d^{10}nl$ ^2L_j states of Cu-like W^{45+}. Comparison RMBPT and COWAN results with recommended NIST data [25].

Level	$E^{(\mathrm{COWAN})}$	$E^{(\mathrm{DF})}$	$E^{(\mathrm{DF+2})}$	$E^{(\mathrm{DF+2+3})}$	$E^{(\mathrm{DF+SD})}$	$E^{(\mathrm{NIST})}$
$4s$ $^2S_{1/2}$	0.0	0.0	0.0	0.0	0.0	0.00
$4p$ $^2P_{1/2}$	773.0	790.2	787.3	787.3	787.4	787.41
$4p$ $^2P_{3/2}$	1618.4	1614.0	1605.9	1605.8	1605.9	1604.21
$4d$ $^2D_{3/2}$	2804.0	2835.6	2820.2	2820.2	2820.3	2819.60
$4d$ $^2D_{5/2}$	2983.3	3012.6	2994.3	2994.2	2994.3	2993.56
$4f$ $^2F_{5/2}$	4279.4	4313.6	4293.5	4293.2	4293.7	4293.4
$4f$ $^2F_{7/2}$	4329.8	4359.6	4337.6	4337.4	4337.8	4337.2
$5s$ $^2S_{1/2}$	7800.8	7810.6	7804.4	7804.1	7804.0	7804.
$5p$ $^2P_{1/2}$	8174.4	8194.2	8187.1	8186.8	8186.8	8186.
$5p$ $^2P_{3/2}$	8574.3	8581.0	8571.4	8571.1	8571.0	8572.
$5d$ $^2D_{3/2}$	9138.6	9163.1	9150.5	9150.3	9150.2	9149.
$5d$ $^2D_{5/2}$	9225.8	9248.9	9234.9	9234.6	9234.6	9235.
$5f$ $^2F_{5/2}$	9801.1	9826.2	9812.6	9812.1	9812.2	9813.
$5f$ $^2F_{7/2}$	9827.9	9852.5	9838.1	9837.7	9837.7	9838.
$5g$ $^2G_{7/2}$	10119.1	10145.5	10131.5	10130.8	10130.8	10131.
$5g$ $^2G_{9/2}$	10130.1	10156.0	10141.8	10141.2	10141.2	10141.
$6s$ $^2S_{1/2}$	11690.8	11703.6	11695.6	11695.2	11695.0	
$6p$ $^2P_{1/2}$	11897.6	11916.9	11908.6	11908.2	11908.1	
$6p$ $^2P_{3/2}$	12118.3	12129.8	12120.1	12119.6	12119.5	
$6d$ $^2D_{3/2}$	12431.3	12452.1	12441.0	12440.6	12440.5	
$6d$ $^2D_{5/2}$	12480.3	12500.4	12488.5	12488.0	12487.9	
$6f$ $^2F_{5/2}$	12792.0	12813.4	12801.8	12801.2	12801.2	12796.
$6f$ $^2F_{7/2}$	12807.7	12829.1	12817.1	12816.5	12816.5	12816.
$6g$ $^2G_{7/2}$	12972.4	12993.8	12981.9	12981.2	12981.1	12980.
$6g$ $^2G_{9/2}$	12979.0	13000.0	12988.0	12987.3	12987.2	12981.
Ion. Pot.		19487.2	19478.5	19477.7	19477.6	19471.1

need to calculate the all-order excitation coefficients using an iterative procedure [39]. The correlation contributions to matrix elements are a linear superposition of quadratic functions of the excitation coefficients. The iteration procedure is terminated when the relative change in the correlation energy in two consecutive iterations is sufficiently small (10^{-5} in the present calculations; see for details Refs. [40–43]). Oscillator strengths and transition rates are evaluated using the all-order matrix elements and wavelengths given in column 4 of Table III. Those wavelengths are obtained from the $E^{(\mathrm{DF+SD})}$ energies listed in Table II. A comparison of the oscillator strengths given in columns 5 and 6 and of the transition rates given in the two last columns ("DF" and "DF+SD" labels) shows that the difference is about 2% - 8%. This difference can be attributed to correlation effects. Wavelengths, weighted oscillator strengths, and weighted radiative transition rates for the $3p^63d^{10}n_1l_1 - 3p^63d^{10}n_2l_2$ transitions of Cu-like tungsten evaluated by the COWAN code are listed in columns 3, 5, and 8 of Table III. The difference of wavelengths calculated by the COWAN code and in the "DF+SD" approximation is less than 1.5%.

The values of oscillator strengths, as well as, transition rates calculated by the COWAN code are between the corresponding values obtained in the DF and DF+SD approximation with a difference about 2% -10%.

Energies and weighted autoionization rates (gA_a) for the core-excited $3p^63d^94l$ $(L_{12}S_{12})4l'(LSJ)$, and $3p^53d^{10}4l$ $(L_{12}S_{12})4l'(LSJ)$ levels calculated using the COWAN and HULLAC codes are given in Table IV. There are 688 levels with different l, l', L_{12}, S_{12}, L, S, and J. We evaluated energies and weighted autoionization rates for all 742 levels. However, only selected results (about 1/10) with the largest values of gA_a are listed in Table IV to illustrate our work. Table IV indicates that the difference between the two codes is about 0.1-0.6 % for energies, and is about 20-60 % for gA_a values. For about half of the 742 levels, the differences between the autoionization rates values are substantially larger. The disagreement among the gA_a values calculated by the COWAN and HULLAC codes for W^{4+}, W^{27+}, and W^{63+} ions was discussed by Safronova et al. in Refs. [27, 30, 44]. In the case of the COWAN code, the gA_a values were calculated with an input of only one energy value for the free

TABLE III: Wavelengths (λ in Å), weighted oscillator strengths (gf), and weighted transition rates(gA_r in s^{-1}) for the $3p^63d^{10}nl_1-3p^63d^{10}nl_2$ transitions of Cu-like tungsten. Oscillator strengths and transition rates are obtained from the COWAN code as well as from the DF and all-order RMBPT approximations.

| Low level | Upper level | Wavelengths (λ in Å) | | Oscillator strengths (gf) | | | Transition rates (gA_r in s^{-1}) | | |
nl, LSJ	nl, LSJ	COWAN	DF+SD	COWAN	DF	DF+SD	COWAN	DF	DF+SD
$4d\ ^2D_{5/2}$	$6f\ ^2F_{7/2}$	10.178	10.181	0.8586	0.8975	0.8647	5.53[13]	5.77[13]	5.56[13]
$4d\ ^2D_{5/2}$	$5f\ ^2F_{7/2}$	14.608	14.613	2.8518	2.9505	2.9296	8.91[13]	9.21[13]	9.15[13]
$4f\ ^2F_{7/2}$	$5g\ ^2G_{9/2}$	17.243	17.231	9.3424	9.5769	9.1386	2.10[14]	2.15[14]	2.05[14]
$4f\ ^2F_{7/2}$	$5d\ ^2D_{5/2}$	20.428	20.422	0.3060	0.2803	0.3026	4.89[12]	4.47[12]	4.84[12]
$5d\ ^2D_{5/2}$	$6f\ ^2F_{7/2}$	27.912	27.918	2.3525	2.4467	2.4596	2.01[13]	2.09[13]	2.11[13]
$5f\ ^2F_{7/2}$	$6g\ ^2G_{9/2}$	31.744	31.751	7.4281	7.5043	7.4345	4.92[13]	4.96[13]	4.92[13]
$5g\ ^2G_{7/2}$	$6f\ ^2F_{5/2}$	37.402	37.448	0.1491	0.1501	0.1537	7.11[11]	7.13[11]	7.31[11]
$5f\ ^2F_{5/2}$	$6d\ ^2D_{3/2}$	38.032	38.048	0.4786	0.4966	0.5107	2.21[12]	2.28[12]	2.35[12]
$4p\ ^2P_{1/2}$	$4d\ ^2D_{3/2}$	49.256	49.191	1.2247	1.2373	1.1534	3.37[12]	3.45[12]	3.18[12]
$4s\ ^2S_{1/2}$	$4p\ ^2P_{3/2}$	61.757	62.272	0.9876	1.0324	0.9646	1.73[12]	1.79[12]	1.66[12]
$4d\ ^2D_{3/2}$	$4f\ ^2F_{5/2}$	67.743	67.869	1.2086	1.2496	1.1758	1.76[12]	1.82[12]	1.70[12]
$4d\ ^2D_{5/2}$	$4f\ ^2F_{7/2}$	74.222	74.431	1.5758	1.6349	1.5425	1.91[12]	1.98[12]	1.86[12]
$5p\ ^2P_{1/2}$	$5d\ ^2D_{3/2}$	103.803	103.793	1.7342	1.6931	1.6492	1.07[12]	1.06[12]	1.02[12]
$5s\ ^2S_{1/2}$	$5p\ ^2P_{3/2}$	129.136	130.381	1.3491	1.3518	1.3180	5.40[11]	5.35[11]	5.17[11]
$5d\ ^2D_{5/2}$	$5f\ ^2F_{7/2}$	165.856	165.799	2.5674	2.5843	2.5400	6.23[11]	6.28[11]	6.16[11]
$6p\ ^2P_{1/2}$	$6d\ ^2D_{3/2}$	187.656	187.822	2.1781	2.1159	2.0864	4.13[11]	4.04[11]	3.95[11]
$6s\ ^2S_{1/2}$	$6p\ ^2P_{3/2}$	233.475	235.578	1.6725	1.6643	1.6430	2.05[11]	2.02[11]	1.98[11]
$6d\ ^2D_{5/2}$	$6f\ ^2F_{7/2}$	304.686	304.346	3.3896	3.4053	3.3808	2.44[11]	2.45[11]	2.44[11]
$5f\ ^2F_{5/2}$	$5g\ ^2G_{7/2}$	315.289	313.867	0.8374	0.8449	0.8345	5.62[10]	5.75[10]	5.65[10]
$5f\ ^2F_{7/2}$	$5g\ ^2G_{7/2}$	344.411	341.211	0.0284	0.0286	0.0283	1.60[09]	1.63[09]	1.62[09]
$6f\ ^2F_{7/2}$	$6g\ ^2G_{7/2}$	609.930	607.356	0.0504	0.0504	0.0501	9.03[08]	9.12[08]	9.06[08]

electron wave functions. The dependence of gA_a on the input energies (200 and 700 Ry) was studied earlier [44]. The difference was about a factor of 2-5 for most of cases. In the HULLAC code, the gA_a values were evaluated for those levels whose energies are below the ionization energy. The first autoionizing state ($3p^63d^94d4f\ ^2G_{7/2}$) appeared at the energy equal to 19488.3 cm^{-1}, while the NIST ionization energy [25] is equal to 19471.1 cm^{-1}. Such a large difference in the determination of the ionization limit by the HULLAC code leads to incorrect gA_a values near the threshold in Cu-like W^{45+}.

A small set of the $3p^63d^94l\ (L_{12}S_{12})4l'(LSJ)$ and the $3p^53d^{10}4l\ (L_{12}S_{12})4l'(LSJ)$ levels calculated using the COWAN and HULLAC codes are listed in Table V to compare with the recommended NIST energy data [26]. We displayed both designations used in the COWAN and HULLAC codes. In the HULLAC code, the level's name has twelve characters, the first four are the name of the parent non-relativistic configuration given in the input file, the next two digits represent the specific relativistic sub-configuration, the next four represent part of the re-coupling scheme used, and the last two are the twice the total J value of the level. The level's name is unique, i.e. for the same definition of configuration the same level name will be used in the final result.

A comparison of the energy values given in columns "COWAN", "HULLAC", and NIST [26] demonstrates excellent agreement of both theoretical results with the recommended NIST values. The best agreement is found for the core-excited states: 0.1% - 0.4% for results in the "COWAN" column and 0.01% - 0.3% for results in the "HULLAC" column. There is a larger disagreement for the singly excited states. The difference between the energies in the "HULLAC" and "NIST" columns is smaller than the difference between energies in the "COWAN" and "NIST" columns. The small difference in the $3p^63d^{10}4l$ energies given in Tables II and V and obtained by the COWAN code is due to the inclusion of a different set of configurations.

The comparison of the results obtained by different methods is very important when only a few experimental measurements are available. We conclude from the comparison of the results given in Tables II, III, IV, and V that the energies values obtained by different codes are in a good agreement (0.1–1%) and that the differences in the transition rates do not exceed 10-20% for largest values of those properties. The comparison of data in the cases where more accurate RMBPT codes are applicable give an assessment of the accuracy the respective method and of the quality of the data obtained in other systems where the RMBPT cannot be used owing to the complexity in the electronic structure. Such a comparison is

TABLE IV: Energies E (in 10^3 cm^{-1}) and weighted autoionization rates gA_a (in s^{-1}) for the doubly excited $3p^63d^94l4l'$ and $3p^53d^{10}4l4l'$ levels calculated using the COWAN and HULLAC codes. The upper indices are used in the Cowan code to differentiate between atomic terms. Designations $3p^63d^9nln'l' = 3dnln'l'$, and $3p^53d^{10}nl = 3pnln'l'$. A[B] means A·10^B.

Level	$E^{(\text{HULLAC})}$	$E^{(\text{COWAN})}$	$gA_a^{(\text{HULLAC})}$	$gA_a^{(\text{COWAN})}$	Level	$E^{(\text{HULLAC})}$	$E^{(\text{COWAN})}$	$gA_a^{(\text{HULLAC})}$	$gA_a^{(\text{COWAN})}$
$3p4s4p\ ^4P_{1/2}$	19493.7	19475.6	1.88[14]	1.69[14]	$3d4f^2\ ^4F_{3/2}$	21599.1	21606.3	3.25[09]	3.13[09]
$3d4d4f\ ^4H_{9/2}$	19516.9	19506.7	1.23[11]	1.30[11]	$3d4f^2\ ^2H_{9/2}$	21680.2	21689.4	1.62[12]	1.29[12]
$3d4d4f\ ^4F^a_{7/2}$	19554.0	19554.3	4.12[11]	3.96[11]	$3d4f^2\ ^4P_{1/2}$	21719.2	21709.8	1.06[12]	1.57[12]
$3d4d4f\ ^2D^e_{3/2}$	19593.6	19581.5	1.88[12]	1.88[12]	$3p4d^2\ ^2F_{5/2}$	21898.8	21825.4	3.08[12]	3.88[12]
$3d4d4f\ ^2D^f_{5/2}$	19679.0	19655.9	1.63[13]	1.16[13]	$3p4p4f\ ^4D^b_{3/2}$	22000.3	21905.7	2.08[11]	1.64[11]
$3d4d4f\ ^2D_{3/2}$	20087.6	20087.3	1.45[12]	1.33[12]	$3p4p4f\ ^2P^b_{1/2}$	22237.6	22121.2	3.46[12]	3.75[12]
$3d4d4f\ ^4P_{1/2}$	20158.4	20152.5	6.40[11]	6.66[11]	$3p4p4d\ ^4P^a_{3/2}$	23318.9	23234.6	1.48[12]	1.14[12]
$3d4d4f\ ^4F^b_{3/2}$	20267.3	20269.9	3.07[11]	3.34[11]	$3p4d4f\ ^4D^b_{7/2}$	23334.7	23210.4	1.09[12]	1.12[12]
$3d4d4f\ ^4H^a_{11/2}$	20275.9	20287.2	2.12[11]	1.91[11]	$3p4d4f\ ^4F^b_{5/2}$	23349.5	23266.6	2.01[12]	1.47[12]
$3p4p^2\ ^4D_{1/2}$	20277.6	20256.0	1.75[14]	1.53[14]	$3p4d4f\ ^4P^a_{1/2}$	23501.7	23370.3	9.95[11]	9.99[11]
$3d4d4f\ ^2H^c_{9/2}$	20280.9	20282.5	4.74[12]	4.21[12]	$3p4d4f\ ^2S^b_{1/2}$	23613.8	23475.2	3.67[13]	3.33[13]
$3d4d4f\ ^4D^c_{3/2}$	20368.8	20358.4	2.26[12]	2.79[12]	$3p4p4f\ ^4D^b_{7/2}$	24500.8	24526.7	3.45[11]	3.26[11]
$3p4s4p\ ^2D^b_{3/2}$	20411.7	20335.9	1.11[13]	1.44[13]	$3p4f^2\ ^4D_{3/2}$	24569.8	24571.3	1.13[12]	1.33[12]
$3p4p4d\ ^4P^a_{3/2}$	20607.4	20506.5	4.00[12]	4.03[12]	$3p4f^2\ ^4F_{7/2}$	24587.9	24592.3	2.04[13]	1.91[13]
$3d4f^2\ ^4D_{3/2}$	21043.4	21031.3	6.48[10]	6.01[10]	$3p4p4f\ ^2P^b_{3/2}$	24685.0	24606.1	3.65[11]	3.26[11]
$3d4f^2\ ^2D_{5/2}$	21139.3	21126.2	3.21[10]	3.07[10]	$3p4d^2\ ^2D_{5/2}$	24696.0	24611.5	6.33[12]	6.64[12]
$3p4p4f\ ^4F^a_{5/2}$	21182.9	21070.6	1.12[12]	1.21[12]	$3p4f^2\ ^4S_{3/2}$	24833.1	24712.6	1.42[12]	1.38[12]
$3d4f^2\ ^2F_{7/2}$	21291.0	21269.9	1.11[14]	2.11[14]	$3p4d4f\ ^4D_{1/2}$	25831.5	25810.3	8.24[12]	8.43[12]
$3p4s4d\ ^4D_{1/2}$	21436.0	21447.7	2.44[12]	2.29[12]	$3p4d4f\ ^4P^a_{1/2}$	25984.2	25971.5	7.59[12]	8.21[12]

especially important for our case, because all numerical data and graphs below are obtained using the COWAN code data. In particular, in Table I, we show configurations that should be used to produce the dielectronic satellite spectra and the (DR) rate coefficients of Cu-like tungsten from Ni-like tungsten. The use of the most complete set of states is very important for an accurate evaluation of the branching ratios. The summation over both non-autoionizing and autoionizing states has to be included. The version of COWAN code in [33] allows us to extract atomic properties in a more convenient way than the HULLAC code for evaluating the branching ratios and the effective emission rate coefficients of the dielectronic satellite lines.

III. DIELECTRONIC SATELLITE SPECTRA

Dielectronic recombination of the Ni-like W^{46+} ion proceeds via electron capture into the intermediate autoionizing states of the Cu-like W^{45+} ion followed by the radiative decay to singly excited bound states:

$$W^{46+}(3p^63d^{10}) + e \rightarrow W^{45+*}(3p^63d^9n_1l_1n_2l_2 + 3p^53d^{10}n_1l_1n_2l_2)$$
$$\downarrow \qquad\qquad \downarrow$$
$$W^{46+}(3p^63d^{10}) + e. \quad W^{45+*}(3p^63d^{10}nl + 3p^63d^94s4l + 3p^63d^94p4l + 3p^63d^94d^2 + 3p^53d^{10}4s^2) + h\nu. \quad (1)$$

An alternative decay channel for the autoionizing level in Eq. (1) is via autoionization, and in this case the system returns to its original state $3p^63d^{10}$ as shown by a vertical arrow in Eq. (1).

Importantly, not all of the doubly excited states listed in the previous section can autoionize. The $3p^63d^94f^2$,

$3p^53d^{10}4d4l$ ($l = p, d$), $3p^53d^{10}4f4l$ ($l = p, d, f$), $3p^63d^94l'nl$, $3p^53d^{10}4l'nl$ (n=5-6), and $3p^63d^95l'nl$, (n=5-7) levels are indeed autoionizing levels. However, the $3p^63d^94d4f$, $3p^53d^{10}4s4p$, $3p^53d^{10}4s4d$, and $3p^53d^{10}4p^2$ configurations are only partly autoionizing, as some of the levels have energies below the ionization

TABLE V: Energies E (in 10^3 cm^{-1}) for the singly excited $3p^63d^{10}4l$ and doubly excited $3p^63d^94l4l'$ and $3p^53d^{10}4l4l'$ levels calculated using the COWAN and HULLAC codes and compared with the recommended NIST data [26]. The upper indices are used in the Cowan code to differentiate between atomic terms. Designations used are: $3p^63d^{10}nln'l' = nl$, $3p^63d^9nln'l' = 3dnln'l'$, and $3p^53d^{10}nl = 3pnln'l'$.

| Levels designations | | Energies in 10^3 cm^{-1} | | | Levels designations | | Energies in 10^3 cm^{-1} | | |
COWAN	HULLAC	COWAN	HULLAC	NIST [26]	COWAN	HULLAC	COWAN	HULLAC	NIST [26]
$4s\ ^2S_{1/2}$	$4s0001..01$	0.0	0.0	0.0	$3d4p^2\ ^4F_{3/2}$	$3d4p4p0205..03$	15412.1	15379.7	15369.
$4p\ ^2P_{1/2}$	$4p0101..01$	773.7	794.5	787.41	$3d4s4d\ ^2P_{3/2}^b$	$3d4p4p0202..03$	15436.6	15422.3	15413.
$4p\ ^2P_{3/2}$	$4p0001..03$	1619.1	1610.1	1604.21	$3d4p^2\ ^2F_{5/2}$	$3d4p4p0203..05$	15444.5	15416.5	15401.
$4d\ ^2D_{3/2}$	$4d0101..03$	2803.7	2827.3	2819.6	$3d4p^2\ ^2D_{5/2}$	$3d4p4p0104..05$	15777.1	15745.8	15738.
$4d\ ^2D_{5/2}$	$4d0001..05$	2983.0	3000.3	2993.55	$3d4p^2\ ^2P_{3/2}$	$3d4p4p0103..03$	15781.6	15751.8	15738.
$4f\ ^2F_{5/2}$	$4f0101..05$	4278.8	4299.2	4293.4	$3p4s^2\ ^2P_{3/2}$	$3p4s4s0101..03$	16088.3	16168.8	16132.
$4f\ ^2F_{7/2}$	$4f0001..07$	4329.2	4342.3	4293.4	$3d4p^2\ ^4P_{1/2}$	$3d4p4p0002..01$	16311.8	16283.5	16276.
$3d4s^2\ ^2D_{5/2}$	$3d4s4s0101..05$	12511.9	12486.1	12482.	$3d4p^2\ ^2F_{5/2}$	$3d4p4p0004..05$	16317.3	16276.4	16276.
$3d4s4p\ ^4F_{3/2}$	$3d4s4p0202..03$	13734.0	13708.9	13708.	$3d4p4d\ ^2P_{1/2}^f$	$3d4p4d0504..01$	16854.9	16866.8	16875.
$3d4s4p\ ^4P_{3/2}$	$3d4s4p0203..03$	13793.6	13778.3	13770.	$3d4p4d\ ^2P_{1/2}^b$	$3d4p4d0501..01$	16883.4	16906.3	16901.
$3d4s4p\ ^4D_{1/2}$	$3d4s4p0201..01$	13800.0	13786.7	13770.	$3d4p4d\ ^4S_{3/2}$	$3d4p4d0505..03$	16888.2	16874.4	16875.
$3d4s4p\ ^4P_{3/2}$	$3d4s4p0102..03$	14054.0	14016.7	14011.	$3d4s4f\ ^4D_{3/2}$	$3d4s4f0101..03$	16915.5	16909.6	16901.
$3d4s4p\ ^2P_{1/2}^a$	$3d4s4p0101..01$	14061.5	14025.5	14023.	$3d4p4d\ ^4F_{3/2}^b$	$3d4p4d0406..03$	17486.3	17468.4	17486.2
$3d4s4p\ ^2P_{3/2}^b$	$3d4s4p0105..03$	14165.0	14144.1	14130.	$3d4s4f\ ^2P_{1/2}^b$	$3d4p4d0405..01$	17492.9	17487.8	17471.2
$3d4s4p\ ^4P_{1/2}$	$3d4s4p0001..01$	14562.1	14503.6	14501.	$3d4p4d\ ^2F_{5/2}^d$	$3d4p4d000c..05$	17708.2	17692.5	17692.
$3d4s4p\ ^4D_{3/2}$	$3d4s4p0002..03$	14589.3	14535.5	14526.	$3p4s4d\ ^2P_{3/2}^a$	$3p4s4d0101..03$	19040.3	19142.2	19092.
$3d4p^2\ ^4F_{3/2}$	$3d4p4p0401..03$	14607.6	14616.4	14596.	$3p4s4d\ ^2P_{1/2}^b$	$3p4s4d0104..01$	19070.0	19170.8	19125.
$3d4s4p\ ^2P_{1/2}^b$	$3d4s4p0004..01$	14700.8	14664.2	14648.	$3p4p^2\ ^2P_{3/2}$	$3p4p4f0705..03$	21127.0	21216.4	21227.
$3d4p^2\ ^2P_{3/2}$	$3d4p4p0302..03$	14866.9	14849.1	14856.	$3p4p4f\ ^2D_{3/2}^c$	$3p4p4f0304..03$	21201.8	21333.5	21275.
$3d4p^2\ ^2S_{1/2}$	$3d4p4p0301..01$	14880.1	14861.4	14846.	$3p4s4f\ ^4G_{5/2}$	$3p4s4f0201..05$	22892.9	22875.0	22831.

potential. Finally, none of the levels of the the doubly excited $3p^63d^94s4l$, $(l = s, p, d, f)$, $3p^63d^94p4l$, $(l = p, d, f)$, $3p^63d^94d^2$, $3p^53d^{10}4s^2$ configurations can autoionize.

During the radiative-stabilization phase of DR, dielectronic satellite lines are emitted when an electron jumps from a doubly excited autoionizing state to a singly or doubly excited bound state. For instance, the radiative transitions from the $3p^63d^94l'nl$, $3p^53d^{10}4l'nl$, and $3p^63d^95l'nl$ to the $3p^63d^{10}nl$ states give rise to satellite lines of the $3d - 4l$, $3p - 4l$, and $3d - 5l$ lines of Cu-like tungsten. Assuming a Maxwellian distribution, the effective emission rate coefficient of a dielectronic satellite line can written as (see, for example, Ref. [45]):

$$C_S^{eff}(j,i) = 3.3 \times 10^{-24} \left(\frac{I_H}{kT_e}\right)^{3/2} \frac{Q_d(j,i)}{g_0}$$
$$\times \exp\left(-\frac{E_S(i)}{kT_e}\right) \text{ photons cm}^3\text{s}^{-1}, \quad (2)$$

where the intensity factor $Q_d(j,i)$ is defined as:

$$Q_d(j,i) = \frac{g(i)A_a(i,i_0)A_r(j,i)}{\sum_{i_0'} A_a(i,i_0') + \sum_k A_r(k,i)}, \quad (3)$$

and I_H is the ionization potential of hydrogen, j is the lower bound state, i is the upper autoionizing state, i_0

is the initial state (i.e., the ground state $3p^63d^{10}$ of the Ni-like ion), and i_0' is the possible final state for autoionization (again, only $3p^63d^{10}$ in this case). The statistical weight of the initial state i_0 is $g_0 = 1$, $g(i)$ is the statistical weight of the doubly excited state, $A_a(i,i_0)$ is the autoionization rate from i to i_0, $A_r(j,i)$ is the radiative transition probability from i to j, $E_S(i)$ is the excitation energy of the autoionizing state i relative to the energy of $3p^63d^{10}$, and T_e is the electron temperature. For some cases, $A_a \gg A_r$ and then Q_d can be estimated as $Q_d(j,i) \approx g(i)A_r(j,i)$.

It follows from Eq. (2) that the intensity of dielectronic satellites depends on the intensity factor $Q_d(j,i)$ and excitation energy $E_S(i)$. The strongest lines with $Q_d(j,i) > 5.0 \times 10^{12}$ s^{-1} are presented in Tables VI and VII for even- and odd-parity initial states, respectively. Since the sum over the final states of autoionization i_0' in Eq. (3) includes only one state, $3p^63d^{10}$, it is in fact reduced to a single rate $A_a(i)$. In addition to the $A_a(i)$ values, Tables VI and VII also present $E_S(i)$, weighted radiative rates $g_iA_r(j,i)$, sums of weighted radiative rates $\sum_k g_iA_r(k,i)$, wavelengths λ for dipole-allowed transitions, relative intensity factors $Q_d(j,i)$, and effective emission rate coefficients $C_S^{eff}(j,i)$. Short designations are used in these tables and in the text below: $3p^63d^{10}nl$

TABLE VI: Autoionization rates (A_a in s^{-1}) and excitation energies (E_S in eV) for the $3p^63d^94lnl'$ and $3p^53d^{10}4lnl'$ states. Wavelengths (λ in Å), weighted radiative rates (gA$_r$ in s^{-1}), intensity factors (Q_d in s^{-1}), and effective emission rate coefficients (C$_S^{\mathrm{eff}}$ in cm^3/s) for transitions between the $3p^63d^{10}nl$ even-parity excited and the $[3p^63d^94lnl' + 3p^53d^{10}4lnl']$ odd-parity autoionization states of Cu-like tungsten. The C$_S^{\mathrm{eff}}$ values were calculated at T$_e$=800 eV. Designations used are: $3p^63d^{10}nl = nl$, $3p^63d^9nln'l' = 3dnln'l'$, and $3p^53d^{10}nln'l' = 3pnln'l'$. The upper indices are used in the Cowan code to differentiate between atomic terms. A[B] means A$\cdot10^B$.

Low level $nl\ LSJ$	Upper level $3lnln'l'\ LSJ$	λ Å	gA$_r$ s^{-1}	ΣgA$_r$ s^{-1}	A$_a$ s^{-1}	E$_S$ eV	Q$_d$ s^{-1}	C$_S^{\mathrm{eff}}$ cm^3/s
$4d\ ^2D_{3/2}$	$3d4d4f\ ^4G_{5/2}^a$	5.8456	1.94[14]	2.66[14]	1.60[14]	54.5	1.52[14]	1.04[-12]
$4d\ ^2D_{3/2}$	$3d4d4f\ ^2D_{5/2}^e$	5.7321	5.35[14]	9.71[12]	2.58[12]	96.5	3.29[14]	2.13[-12]
$4d\ ^2D_{3/2}$	$3d4d4f\ ^2F_{5/2}^i$	5.7286	1.22[15]	1.23[15]	1.69[14]	97.8	5.51[14]	3.57[-12]
$4d\ ^2D_{5/2}$	$3d4d4f\ ^2D_{5/2}^h$	5.9024	6.54[14]	6.65[14]	4.46[13]	56.3	1.88[14]	1.28[-12]
$4d\ ^2D_{5/2}$	$3d4d4f\ ^2G_{7/2}^e$	5.8938	3.25[14]	3.31[14]	1.46[14]	59.4	2.53[14]	1.72[-12]
$4d\ ^2D_{5/2}$	$3d4d4f\ ^2F_{7/2}^a$	5.7297	1.14[15]	1.15[15]	3.22[13]	119.6	2.09[14]	1.32[-12]
$4d\ ^2D_{3/2}$	$3d4d4f\ ^2F_{5/2}^a$	5.6820	1.54[14]	1.63[14]	2.20[14]	115.6	1.37[14]	8.68[-13]
$4d\ ^2D_{5/2}$	$3d4d5f\ ^2F_{7/2}^i$	4.4513	6.35[14]	7.46[14]	7.25[13]	740.9	2.77[14]	8.04[-13]
$4d\ ^2D_{5/2}$	$3d4d6f\ ^2F_{7/2}^i$	3.9295	3.87[14]	4.56[14]	3.34[13]	1110.7	1.43[14]	2.61[-13]
$4s\ ^2S_{1/2}$	$3p4s4d\ ^4D_{3/2}$	4.6601	2.54[14]	2.96[14]	2.15[12]	246.4	7.17[12]	3.86[-14]
$4s\ ^2S_{1/2}$	$3p4s4d\ ^2D_{3/2}^b$	4.6181	9.70[12]	5.10[13]	1.11[13]	270.6	4.51[12]	2.35[-14]
$4d\ ^2D_{5/2}$	$3p4d^2\ ^2F_{7/2}$	5.2726	1.32[14]	1.36[14]	6.68[12]	307.0	3.72[13]	1.85[-13]
$4d\ ^2D_{5/2}$	$3p4p4f\ ^4D_{3/2}^a$	5.2627	2.49[13]	2.58[12]	7.92[12]	311.4	2.30[13]	1.14[-13]
$4d\ ^2D_{5/2}$	$3p4p4f\ ^4F_{7/2}^b$	5.2609	6.53[13]	7.17[13]	6.99[12]	312.3	2.86[13]	1.42[-13]
$4d\ ^2D_{5/2}$	$3p4p4f\ ^2F_{5/2}^a$	5.2377	7.35[13]	8.82[13]	5.00[13]	322.7	5.68[13]	2.77[-13]
$4d\ ^2D_{5/2}$	$3p4p4f\ ^2D_{5/2}^d$	5.2277	6.10[13]	6.70[13]	2.94[13]	327.2	4.42[13]	2.15[-13]
$4d\ ^2D_{5/2}$	$3p4p4f\ ^2F_{7/2}^a$	5.2143	1.13[14]	1.54[13]	2.74[13]	333.3	1.06[14]	5.10[-13]
$5g\ ^2G_{9/2}$	$3p4s5g\ ^2H_{11/2}^a$	6.1858	1.69[14]	4.36[14]	1.12[13]	845.6	3.98[13]	1.01[-13]
$5g\ ^2G_{9/2}$	$3p4d5g\ ^2H_{11/2}^a$	5.2284	4.21[14]	6.88[14]	1.85[13]	1212.5	1.02[14]	1.65[-13]
$6g\ ^2G_{7/2}$	$3p4d6g\ ^2H_{9/2}^a$	5.2218	4.51[14]	7.27[14]	2.47[13]	1567.8	1.14[14]	1.18[-13]
$6g\ ^2G_{9/2}$	$3p4d6g\ ^2H_{11/2}^a$	5.2242	9.87[14]	1.15[15]	2.80[13]	1567.5	2.22[14]	2.29[-13]
$6g\ ^2G_{9/2}$	$3p4d6g\ ^2H_{11/2}^a$	4.6351	8.12[14]	1.15[15]	2.80[13]	1869.1	1.83[14]	1.29[-13]
$3d4p4f\ ^4G_{9/2}^b$	$3d4p5g\ ^4G_{11/2}^b$	6.8848	2.25[14]	3.00[14]	1.59[12]	675.6	1.34[13]	4.23[-14]
$3d4p4f\ ^2D_{5/2}^d$	$3d4d5f\ ^2F_{7/2}^a$	14.5584	2.51[13]	1.24[14]	2.10[14]	814.3	2.34[13]	6.17[-14]
$3d4d^2\ ^4D_{3/2}$	$3d4d5f\ ^4G_{5/2}^a$	14.1012	4.72[13]	1.07[14]	6.43[13]	793.0	3.70[13]	1.00[-13]
$3d4d^2\ ^2D_{3/2}$	$3d4d5f\ ^2F_{5/2}^a$	13.9920	4.43[13]	1.52[14]	1.65[14]	811.5	3.84[13]	1.02[-13]
$3d4d^2\ ^2D_{5/2}$	$3d4d5f\ ^2F_{7/2}^a$	14.3053	4.95[13]	1.24[14]	2.10[14]	814.3	4.61[13]	1.22[-13]

$= nl$, $3p^63d^9nln'l' = 3dnln'l'$, $3p^53d^{10}nln'l' = 3pnln'l'$. The restriction $Q_d(j, i) > 5.0\times10^{12}$ s^{-1} leaves only a few dozen of lines out of the total of 2.0×10^6 transitions, and most of these lines are due to the one-electron $4l - 3d^94lnl'$, $4l - 3p^54lnl'$ transitions with $n = 4$–5.

The value of the effective emission rate coefficient C_S^{eff} is larger for the $4l - 3d^94lnl'$ transitions than for the $4l - 3p^54lnl'$ transitions by one to two orders of magnitude. In the five last lines of Tables VI and VII, we list transitions from the doubly excited non-autoionising states. The wavelengths of these transitions (40 Å - 70 Å) are larger than the wavelengths of transitions from the singly excited states (5 Å -6 Å) by a factor of 10. The effective emission rate coefficient C_S^{eff} de-

pends on the intensity factor Q_d and excitation energy E_S ($C_S^{\mathrm{eff}} \simeq Q_d(j, i) \times \exp\left(-\frac{E_S(i)}{kT_e}\right)$). Therefore, transitions with a similar value of C_S^{eff} may have have significantly different values of E_S and Q_d. For example, the values of E_S in the three last transitions of Table VII are smaller by a factor of 5-30 than the E_S values of the $3d^94s4f - 3d^94s5g'$ transitions in lines 4-5 from the bottom of Table VII. However, the Q_d values of these transitions are larger than a factor of 10 than the Q_d values of transitions in three last lines of Table VII. Final values of the effective emission rate coefficient C_S^{eff} for those 5 transitions are the same order of magnitudes.

TABLE VII: Autoionization rates (A_a in s^{-1}) and excitation energies (E_S in eV) for the $3p^63d^94lnl'$ and $3p^53d^{10}4lnl'$ states. Wavelengths (λ in Å), weighted radiative rates (gA_r in s^{-1}), intensity factors (Q_d in s^{-1}), and effective emission rate coefficients (C_S^{eff} in cm^3/s) for transitions between the $3p^63d^{10}nl$ odd-parity excited states and the $[3p^63d^94lnl' + 3p^53d^{10}4lnl']$ eve-parity autoionization states of Cu-like tungsten. The C_S^{eff} values were calculated at T_e=800 eV. Designations used are: $3p^63d^{10}nl = nl$, $3p^63d^9nln'l' = 3dnln'l'$, and $3p^53d^{10}nln'l' = 3pnln'l'$. The upper indices are used in the Cowan code to differentiate between atomic terms. A[B] means A·10^B.

Low level nl LSJ	Upper level $3lnln'l'$ LSJ	λ Å	gA_r s^{-1}	ΣgA_r s^{-1}	A_a s^{-1}	E_S eV	Q_d s^{-1}	C_S^{eff} cm^3/s
$4f\ ^2F_{5/2}$	$3d4f^2\ ^2G_{7/2}$	5.9021	1.18[15]	1.32[15]	5.27[14]	217.2	9.01[14]	5.02[-12]
$4f\ ^2F_{5/2}$	$3d4f^2\ ^2G_{7/2}$	5.7497	1.43[15]	1.43[15]	3.80[14]	272.9	9.73[14]	5.06[-12]
$4f\ ^2F_{7/2}$	$3d4f^2\ ^2G_{9/2}$	5.7286	3.01[15]	3.01[15]	8.13[14]	287.1	2.20[15]	1.12[-11]
$5f\ ^2F_{5/2}$	$3d4f5f\ ^2G_{7/2}^a$	5.6988	3.25[15]	3.47[15]	2.33[14]	976.5	1.14[15]	2.45[-12]
$5f\ ^2F_{7/2}$	$3d4f5f\ ^2G_{9/2}^a$	5.8823	1.38[15]	1.52[15]	1.07[14]	912.0	5.71[14]	1.34[-12]
$6h\ ^2H_{9/2}$	$3d4f6h\ ^2I_{11/2}^a$	5.6862	4.71[15]	4.94[15]	9.13[13]	1378.5	8.54[14]	1.12[-12]
$4p\ ^2P_{3/2}$	$3p4p4d\ ^2D_{3/2}^a$	5.2651	1.30[14]	1.40[14]	1.55[14]	141.5	1.06[14]	4.27[-12]
$4p\ ^2P_{3/2}$	$3p4p4d\ ^2P_{3/2}^a$	5.2570	6.72[13]	7.08[13]	2.02[13]	145.1	3.58[13]	1.39[-12]
$4p\ ^2P_{3/2}$	$3p4p4d\ ^2D_{5/2}^f$	5.2509	3.19[14]	3.25[14]	1.01[13]	147.8	5.01[13]	1.89[-12]
$4p\ ^2P_{3/2}$	$3p4p4d\ ^2D_{5/2}^e$	5.2245	4.05[13]	4.64[13]	2.44[13]	159.7	3.08[13]	1.03[-12]
$4p\ ^2P_{3/2}$	$3p4s4p\ ^2P_{1/2}^b$	5.3470	2.41[13]	2.59[13]	1.33[13]	105.4	1.22[13]	7.04[-13]
$4p\ ^2P_{3/2}$	$3p4s4p\ ^2D_{3/2}^b$	5.3460	3.15[13]	3.53[13]	4.05[12]	105.8	9.90[12]	5.68[-13]
$4f\ ^2F_{5/2}$	$3p4s4f\ ^4D_{3/2}$	6.2562	1.83[13]	2.09[13]	2.23[12]	97.8	5.46[12]	3.40[-13]
$4f\ ^2F_{5/2}$	$3p4s4f\ ^2D_{3/2}^a$	6.2391	3.01[13]	3.31[13]	1.74[12]	103.3	5.23[12]	3.08[-13]
$4f\ ^2F_{5/2}$	$3p4d4f\ ^2G_{7/2}^a$	5.2414	2.74[14]	2.88[14]	2.63[13]	481.4	1.16[14]	1.55[-13]
$4f\ ^2F_{7/2}$	$3p4p4d\ ^4G_{9/2}$	6.4695	1.53[12]	3.97[12]	1.26[12]	38.8	1.16[12]	1.30[-13]
$4f\ ^2F_{7/2}$	$3p4s4f\ ^2G_{9/2}^a$	6.2372	7.51[13]	7.82[13]	2.06[11]	110.1	1.93[12]	1.06[-13]
$4f\ ^2F_{7/2}$	$3p4s4f\ ^2F_{7/2}^a$	6.2188	8.17[13]	8.45[13]	2.65[11]	116.0	2.00[12]	1.04[-13]
$4f\ ^2F_{7/2}$	$3p4s4f\ ^2D_{5/2}^a$	6.2182	6.72[13]	8.83[13]	4.79[11]	116.2	2.12[12]	1.10[-13]
$3d4s4f\ ^2H_{11/2}^a$	$3d4s5g\ ^2I_{13/2}^a$	16.8305	2.28[14]	3.13[14]	4.76[12]	405.4	4.00[13]	1.76[-13]
$3d4s4f\ ^2H_{11/2}^k$	$3d4s5g\ ^2I_{13/2}^a$	16.8453	3.01[14]	3.13[14]	4.76[12]	471.7	5.29[13]	2.15[-13]
$3p4p^2\ ^2P_{3/2}$	$3p4p4d\ ^4F_{5/2}^b$	48.6750	7.05[12]	7.72[12]	1.00[12]	23.7	3.08[12]	4.03[-13]
$3p4s4d\ ^4F_{7/2}$	$3p4p4d\ ^4F_{9/2}^b$	60.2351	7.11[12]	1.76[13]	2.52[12]	128.3	4.19[12]	1.92[-13]
$3p4p^2\ ^4D_{7/2}$	$3p4p4d\ ^2G_{9/2}^b$	70.8680	7.22[12]	1.46[13]	4.25[12]	155.2	5.37[12]	1.87[-13]

One can see from Tables VI and VII that in W^{45+}, in contrast to Na-like W^{63+} [44] and Ag-like Xe^{7+} [46], there are a large number of transitions with non-autoionizing doubly excited lower states. In the case of Na-like W^{63+}, only singly excited states are non-autionozing, none of the doubly excited states are non-autoionizing. In the case of Ag-like Xe^{7+}, it was found that about twenty doubly excited states are non-autoionizing. In our case of Cu-like W^{45+}, we found a very large number non-autoionizing doubly excited states (about 430 states)

Strong mixing between some of the doubly excited configurations was already noted in Refs. [44, 46]. Strong mixing of some configurations also occurs in W^{45+}. This effect is exemplified by the $4d\ ^2D_{5/2} - 3p^54p4f\ ^2F_J$ and $4d\ ^2D_{5/2} - 3p^54p4f\ ^2D_J$ transitions in lines 11-15 from the bottom of Table VI. The large intensity fac-

tors Q_d for these transitions are due to the mixing between the $3p^54p4f$ and $3p^54d^2$ configurations. The mixing between the $3p^54p4d$ and $3p^54s4f$ configurations is responsible for the non-zero value for the Q_d value of the $4f\ ^2F_{7/2} - 3p^54p4d\ ^4G_{9/2}$ transition displayed by the line 9 from bottom of Table VII.

The strongest lines shown in the bottom left panel of Fig. 1 result from the $3d^{10}4d\ ^2D_{5/2} - 3d^94d4f\ ^2D_{5/2}^g$ ($\lambda = 5.722$ Å), $3d^{10}4d\ ^2D_{3/2} - 3d^94d4f\ ^2F_{5/2}^i$ ($\lambda = 5.729$ Å), $3d^{10}4f\ ^2F_{7/2} - 3d^94f^2\ ^2G_{9/2}$ ($\lambda = 5.729$ Å), and $3d^{10}4d\ ^2D_{5/2} - 3d^94d4f\ ^2G_{7/2}^e$ ($\lambda = 5.894$ Å) transitions. Those four lines are the satellite lines to the strong lines of the $3d^{10} - 3d^94f$ resonance transitions of Ni-like tungsten ($\lambda = 5.6893$ Å for the $3d_{3/2}4f_{5/2}$ line and $\lambda = 5.8693$ Å for the $3d_{5/2}4f_{7/2}$ line [26]). It should
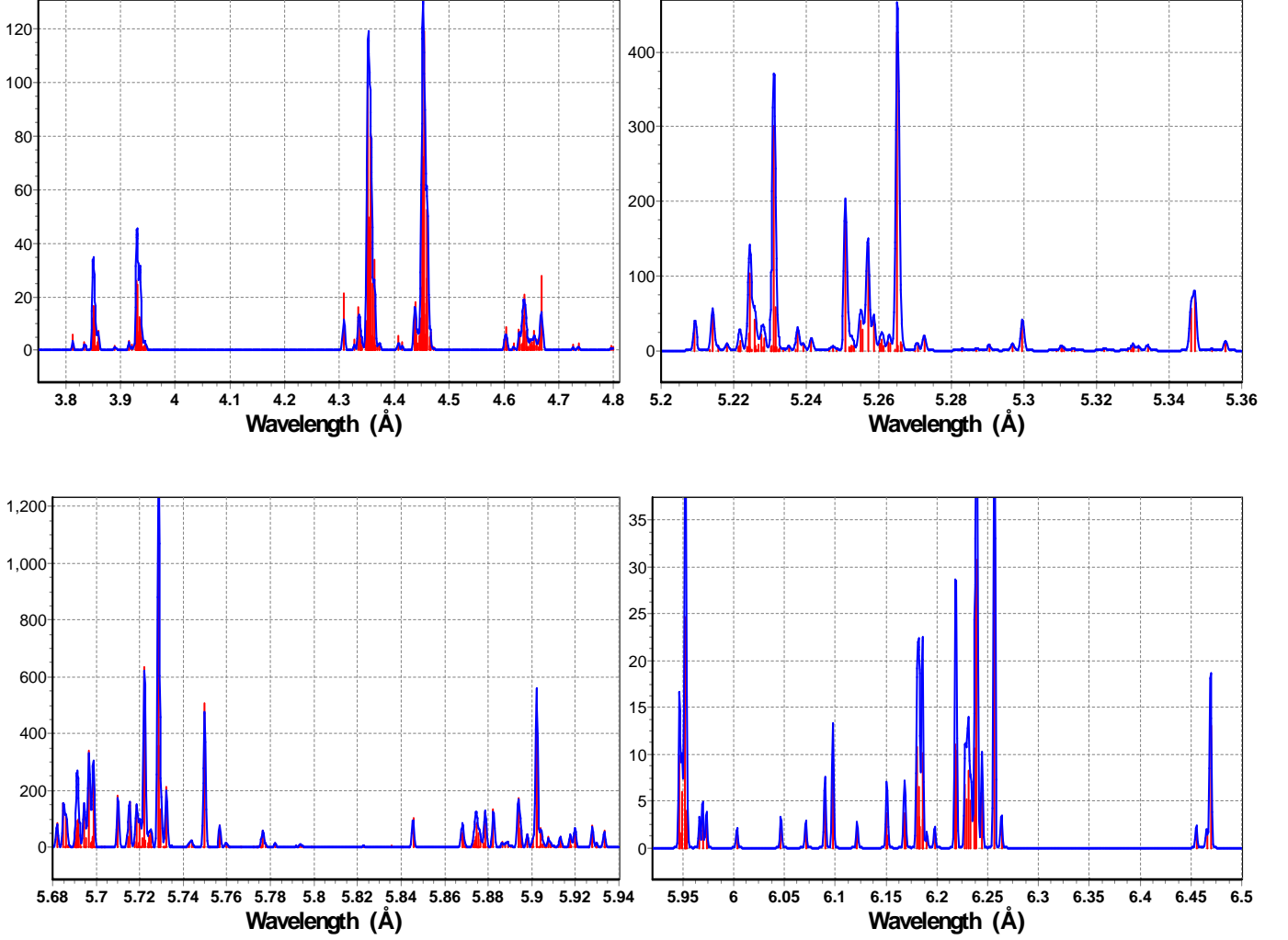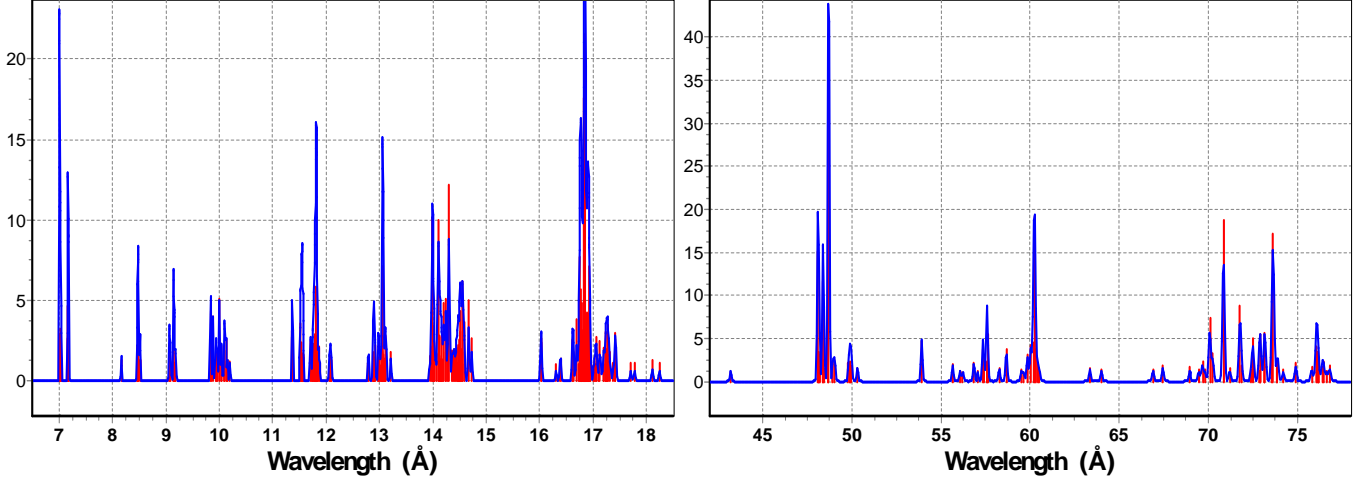
FIG. 1: (Color online) Synthetic spectra of dielectronic satellite lines for transitions between the $3p^63d^{10}nl$ singly excited states and the $[3p^63d^9n_1l_1n_2l_2 + 3p^53d^{10}n_1l_1n_2l_2]$ autoionizing states for Cu-like tungsten at $T_e = 800$ eV. A resolving power, R $= \lambda/\Delta\lambda = 1000$, 5000, 5000, and 2000, respectively, is assumed to produce a Gaussian profile. The scale of the ordinate is in units of 10^{-14} cm^3/s.

be noted that the synthetic spectra shown in the bottom left panel of Fig. 1 result from the $3d^{10}4d - 3d^94d4f$ and $3d^{10}4f - 3d^94f^2$ transitions only. Resulting contribution from the 120 transitions are displayed in this synthetic spectra.

The synthetic spectra shown in the top right panel of Fig. 1 result from the $3p^64p - 3p^54p4d$, $3p^64d - 3p^54d^2$ and $3p^64f - 3p^54d4f$ transitions only. Resulting contribution from the 80 transitions are displayed in this synthetic spectra. The strongest lines shown in the top right panel of Fig. 1 result from the $3p^64p$ $^2P_{1/2} - 3p^54p4d$ $^2P^a_{1/2}$ ($\lambda = 5.231$ Å) and $3p^64p$ $^2P_{1/2} - 3p^54p4d$ $^2D^a_{1/2}$ ($\lambda = 5.265$ Å) transitions. Those two lines are the satellite lines to the strong lines of the $3p^6 - 3p^54d$ resonance transitions of Ni-like tungsten ($\lambda = 5.2004$ Å for the $3p_{3/2}4d_{5/2}$ line and

$\lambda = 5.2533$ Å for the $3p_{3/2}4d_{3/2}$ line [26]). In the top left panel of Fig. 1, the spectra around the strongest lines $3p^64d$ $^2D_{5/2} - 3d^94d5f$ $^2F_{7/2}$ ($\lambda = 4.352$ Å) and $3p^64f$ $^F_{7/2} - 3d^94f5f$ $^2G_{9/2}$ ($\lambda = 4.455$ Å) are satellite spectra to the line of the $3p^6 - 3d^95f$ resonance transitions of Ni-like tungsten ($\lambda = 4.4027$ Å for the $3d^95f$ line [26]).

The satellite spectra of the two resonance line in Ni-like tungsten located at $\lambda = 5.953$ Å ($3d_{5/2}4f_{5/2}$ line)[47] and $\lambda = 6.1518$ Å ($3p_{3/2}4s_{1/2}$ line) [26] are shown in the bottom right panel of Fig. 1. The strongest satellite lines correspond to the $3d^{10}4f$ $^2F_{7/2} - 3d^94f^2$ $^2G_{9/2}$ transition ($\lambda = 5.952$ Å) and the $3p^64f$ $^2F_{5/2} - 3p^54s4f$ $^2D^a_{3/2}$ transition ($\lambda = 6.239$ Å).

FIG. 2: (Color online) Synthetic spectra of dielectronic satellite lines for transitions between the $[3p^63d^94p4l + 3p^63d^94d^2 + 3p^53d^{10}4s^2]$ doubly excited non-autoionizing states and the $[3p^63d^9n_1l_1n_2l_2 + 3p^53d^{10}n_1l_1n_2l_2])$ autoionizing states for Cu-like tungsten at $T_e = 800$ eV. A resolving power, R $= \lambda/\Delta\lambda = 500$ is assumed to produce a Gaussian profile. The scale of the ordinate is in units of 10^{-14} cm^3/s.

The strongest lines shown in the two panels of Fig. 2 result from the transitions between the non-autoionizing $3d^94s4f$, $3d^94p4f$, and $3d^94p^2$ doubly excited states and the autoionizing $3d^94s5g$ and $3d^94d4f$ doubly excited states. The wavelengths of the twenty $3d^94p4f$ $^{2,4}L_J$ - $3d^94d4f$ $^{2,4}L'_{J'}$ lines are in the narrow range of $\lambda = 47.63$ Å - $\lambda = 50.61$ Å. The values of effective emission rate coefficient $C_S^{eff}(3d^94p4f$ $^{2,4}L_J$ - $3d^94d4f$ $^{2,4}L'_{J'})$ are about 10–40 in units of 10^{-14} cm^3/s that is smaller by a factor of 10–50 than the C_S^{eff} for lines displayed in the bottom left panel of Fig. 1.

IV. DIELECTRONIC RECOMBINATION RATE COEFFICIENTS FOR EXCITED STATES

The DR rate coefficients for excited states are obtained by summation of the effective emission rate coefficients $C_S^{eff}(j,i)$ (Eq. (2)) for DR processes through all possible intermediate doubly excited states:

$$\alpha_d(i_0, j) = \sum_i C_S^{eff}(j,i). \qquad (4)$$

For the DR process described by Eq. (1), one has to calculate $\alpha_d(i_0, j)$ with $i_0 = 3p^63d^{10}$ and all possible autoionizing doubly excited states j of W^{45+} with energies larger than the $3p^63d^{10}$ threshold $I_{th} = 19471,100$ cm^{-1} [25]. Among the doubly excited $3p^63d^94f^2$, $3p^53d^{10}4d4l$ $(l = p, d)$, $3p^53d^{10}4f4l$ $(l = p, d, f)$, $3p^63d^94l'nl$, $3p^53d^{10}4l'nl$ $(n$=5-6), and $3p^63d^95l'nl$, $(n$=5-7) states, 6245 states of even parity and 4738 states of odd parity have energies above I_{th}.

The sum over i in Eq. (4) includes the $3p^63d^94l'nl$ with $n = 5$–6 and $n = 4$, $l' = l = f$ (3728 levels),

the $3p^53d^{10}4l'nl$ n=5-6 and $n = 4$, $l' = d, f$, $l = p, d, f$, (2610 levels), and the $3p^63d^95l'nl$ with n=5-7 (4645 levels) doubly excited, autoionizing states. In Fig. 3, we illustrate the contributions of the $3p^63d^94l'nl$, $3p^53d^{10}4l'nl$, and the $3p^63d^95l'nl$ states to the DR rate coefficients $\alpha_d(3p^63d^{10}, j)$ for the $j = 3p^63d^{10}nl$ ^2L_J states as a function of T_e in Cu-like tungsten. It should be noted that we use an abbreviated notation to label the curves in Fig. 3: $3dnl'nl"$ instead of $3p^63d^9nl'nl"$, $3pnl'nl"$ instead of $3p^53d^{10}nl'nl"$, and nl instead of $3p^63d^{10}3d^{10}nl$.

In order to estimate the contributions from the high-n autoionizing states to the DR rate coefficients associated with excited states, i. e. sum over i with $n > 6$ for $3p^63d^94l'nl$ and $3p^53d^{10}4l'nl$ autoionizing states and with $n > 7$ for the $3p^63d^95l'nl$ autoionizing states, we use empirical scaling laws [48], which can only be implemented to include one-electron $3d - np$, $3d - nf$, $3p - ns$, and $3p - nd$ dipole transitions. The contributions from the high-n states appear for the first low-lying configurations $3p^63d^{10}4l$ and $3p^63d^{10}5l$. For these configurations, the $4l - 3d4lnp$, $4l - 3d4lnf$, $4l - 3p4lns$, $4l - 3p4lnd$ transitions with $n > 6$ and $l = s, p, d, f$ are included, as well as the $5l - 3d5lnp$, $5l - 3d5lnf$ transitions with $n > 7$ and $l = s, p, d, f, g$ are considered.

To estimate $Q_d(j,i)$ in Eq.(3) for autoionization states i with high principal quantum number n for the $3d4dnp$ and $3d4dnf$ configurations and for the $3d - np$ and $3d - nf$ dipole transitions, we used our calculated data for $n = 6$ and the $1/n^3$ scaling law [48] for rates A_a and A_r (see, for details, Refs. [27, 28, 30]). In order to obtain the energies of the $3d4dnf$ $^{2,4}L_J$ states as a function of n, the following asymptotic formula is proposed (see Refs. [49, 50]).
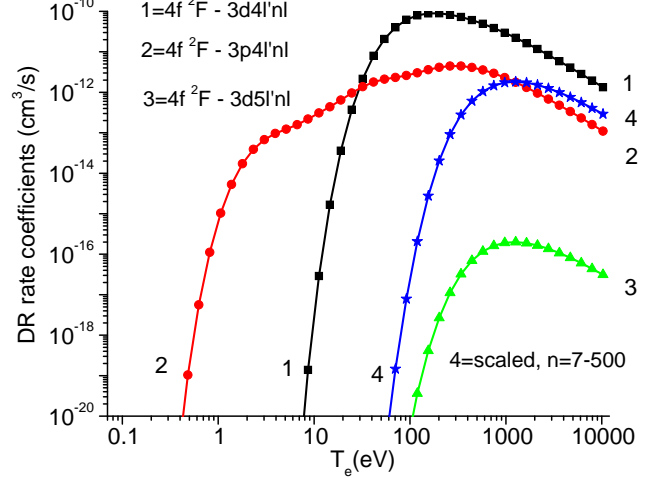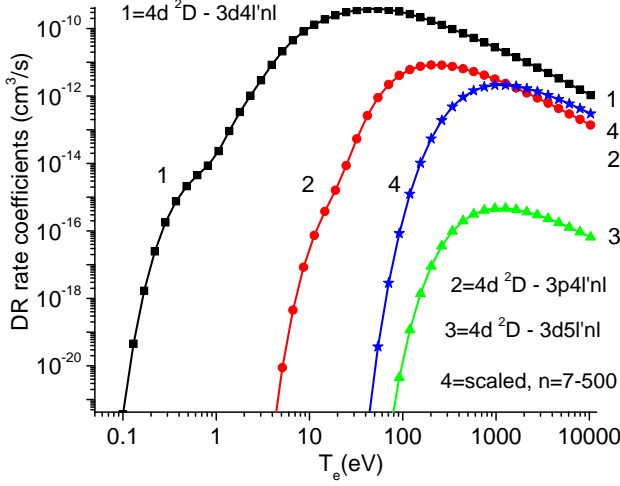
FIG. 3: (Color online) Contribution of the $3p^6 3d^9 4l'nl$ (n=4–6), $3p^5 3d^{10} 4l'nl$ (n=4–6), and $3p^6 3d^9 5l'nl$ (n=5–7) configurations to the DR rate coefficients $\alpha_d(3p^6 3d^{10}, j)$ for the $j = 3p^6 3d^{10} nl\ ^2L_J$ states as a function of T_e in Cu-like tungsten. Curve "4" represents the data calculated using scaling formula for n from 7 to 500 (see text for more details).
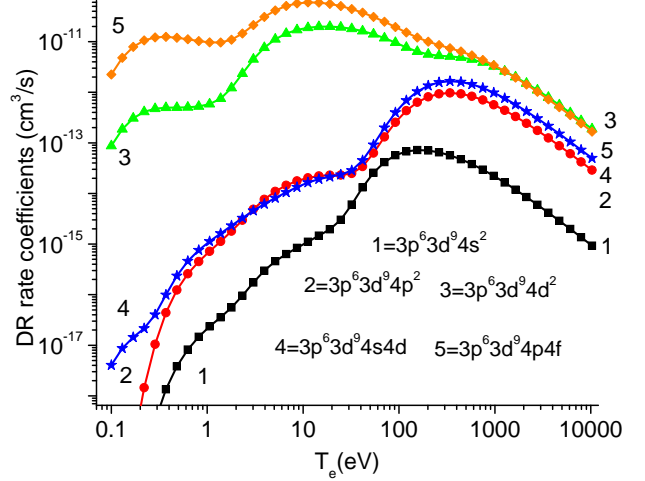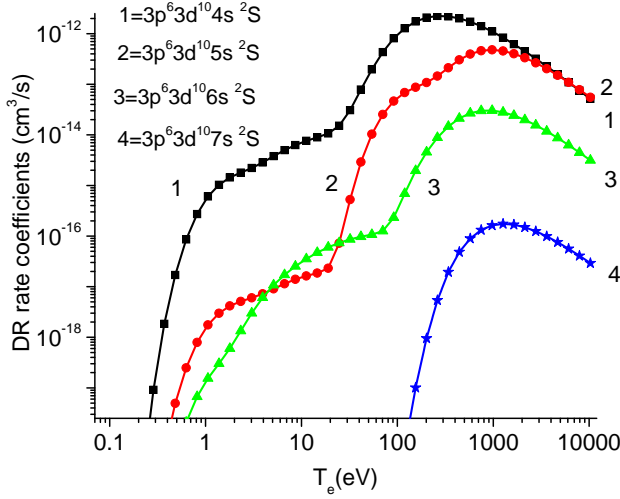

FIG. 4: (Color online) DR rate coefficients $\alpha_d(3p^6 3d^{10}, j)$ for the $j = 3p^6 3d^{10} ns\ ^2S$ and $j = 3p^6 3d^9 4l4l'$ states as a function of T_e in Cu-like tungsten.

Using these scaling formulas for $A_a(3p^6 3d^9 4dnf\ ^{2,4}L_J)$ and $A_r\left(3p^6 3d^{10} 4d\ ^2D_{3/2} - 3p^6 3d^9 4dnf\ ^{2,4}L_J\right)$, we calculated $Q_d(3p^6 3d^{10} 4d\ ^2D_{3/2} - 3p^6 3d^9 4dnf\ ^{2,4}L_J\ )$ as a function of n and then the sums over n for $\alpha_d(3p^6 3d^{10}, 3p^6 3d^{10} 4d\ ^2D_{3/2})$ vs. T_e.

The results of the calculations for the $\alpha_d(3p^6 3d^{10}, j)$ with $j = 3p^6 3d^{10} 4d\ ^2D$ and $j = 3p^6 3d^{10} 4f\ ^2F$ terms are shown in two panels of Fig. 3. The contribution of the scaled data from $n = 7$ up to $n = 500$ for the combined contributions from the autoionizing $3p^6 3d^9 4l'nl$, $3p^5 3d^{10} 4l'nl$, and $3p^6 3d^9 5l'nl$ configurations is presented by curve '4' (cf. curve labeled 'scaled') in Fig. 3. The

dependence of these results on the upper limit of n was also investigated. We found that there is a small difference for low temperature (1% for $T_e = 200$ eV) when $n = 500$ is taken to be the upper limit instead of $n = 20$. The difference increases for high temperatures reaching 8% for $T_e = 2100$ eV. Scaled curves '4' give a larger contribution to $\alpha_d(3p^6 3d^{10}, j)$ than curves '2', describing the $3p^5 3d^{10} 4l'nl$ contribution at $T_e = 2100$ eV (left panel of Fig. 3) and at $T_e = 1300$ eV (right panel of Fig. 3). The importance of these contributions is evident from both panels of Fig. 3.

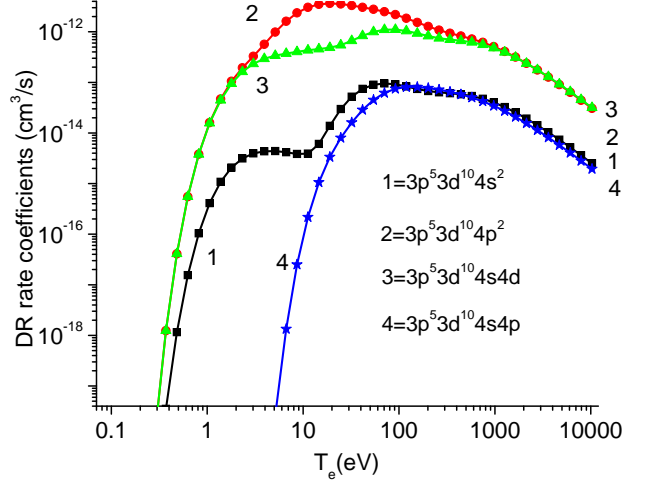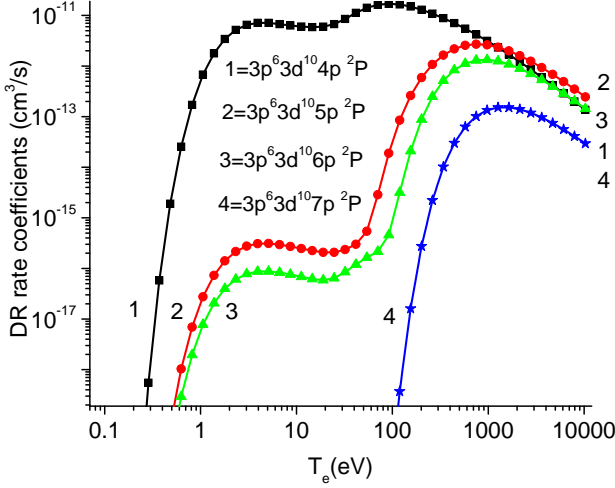The energies E_s may strongly affect the $C_S^{eff}(j, i)$ val-

FIG. 5: (Color online) DR rate coefficients $\alpha_d(3p^63d^{10},j)$ for the $j = 3p^63d^{10}np$ ^2P and $j = 3p^53d^{10}4l4l'$ states as a function of T_e in Cu-like tungsten

ues (see Eq. (2)). The E_s values for the $3p^63d^95l'nl$ autoionizing configurations are larger than the E_s values for the $3p^63d^94l'nl$ and $3p^53d^{10}4l'nl$ autoionizing configurations, which leads to a smaller contribution to the $C_S^{eff}(j,i)$ values of the $3p^63d^95l'nl$ configurations, as described by curve '3' in both panels of Fig. 3).

The calculated values of $\alpha_d(3p^63d^{10},j)$ as a function of T_e in Cu-like tungsten are presented in Figs. 4 and 5. In five panels of Figs. 4 and 5 we present the DR rate coefficients $\alpha_d(3p^63d^{10},j)$ with $j = 3p^63d^{10}ns$ ^2S and $j = 3p^63d^{10}np$ ^2P. In right panels of Figs. 4 and 5, we display the results of the DR rate coefficients for the doubly excited non-autoionizing states: $3p^63d^94s^2$, $3p^63d^94p^2$, $3p^63d^94d^2$, $3p^63d^94s4d$, $3p^63d^94p4f$ $3p^53d^{10}4s^2$ $3p^53d^{10}4p^2$, $3p^53d^{10}4s4d$,and $3p^53d^{10}4s4p$.

The electron temperature for these plots varies from T_e=0.1 eV to $T_e = 10$ keV. In order to decrease the number of curves shown, we summed the results for the doublets $[^2P_{1/2} + {}^2P_{3/2}]$, $[^2D_{3/2} + {}^2D_{5/2}]$, $[^2F_{5/2} + {}^2F_{7/2}]$, $[^2G_{7/2} + {}^2F_{9/2}]$, and $[^2H_{9/2} + {}^2H_{11/2}]$. One can see from Figs. 4 and 5 that the largest values of $\alpha_d(3p^63d^{10},j)$ happens for $j = 3p^63d^{10}4d$ ^2D when $\alpha_d = 3.85\times10^{-10}$ cm^3/s at $T_e = 54$ eV (see curve '1' on the top right panel of Fig. 4). Increasing n in $j = 3p^63d^{10}nl$ ^2L leads to a shift of a given curve's maximum toward larger electron temperature; T_e=50 eV for $n = 4$, up T_e=900 - 1300 eV for $n = 5$–7 (see Fig. 4). Some curves have two maxima, one at T_e=4-5 eV and the second near T_e=750-1300 eV (see for example, the curves on the top left panel of Fig. 5).

The contributions from the doubly excited, non-autoionizing $3p^63d^94s^2$, $3p^63d^94p^2$, $3p^63d^94d^2$, $3p^63d^94s^2$, $3p^63d^94s4d$, $3p^63d^94p4f$, $3p^63d^94s4p$, $3p^63d^94s4f$, $3p^63d^94p4d$, $3p^63d^94d4df$, $3p^53d^{10}4s^2$,
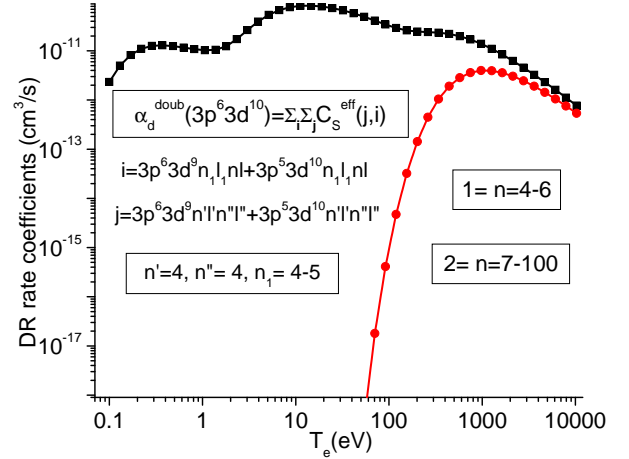

FIG. 6: (Color online) Sum of the contributions from the doubly excited, non-autoionizing $3p^63d^94l'4l$ and $3p^53d^{10}4l'4l$ configurations to the total DR rate coefficients $\alpha_d(3p^63d^{10})$ as a function of T_e in Cu-like tungsten.

$3p^53d^{10}4p^2$, $3p^53d^{10}4s4d$, and $3p^53d^{10}4s4p$ configurations are illustrated in the bottom right panel of Fig. 4 and in the bottom panels of Fig. 5. To obtain $\alpha_d(3p^63d^{10},j)$ for the curves shown in these figures we sum the $\alpha_d(3p^63d^{10})$ evaluated for every transitions included in those configurations. For example, there are 788 and 7771 transitions from non-autoionizing $3p^53d^{10}4s^2$ and $3p^53d^{10}4s4p$ states, respectively. The curves '1' and '4' displayed at the bottom right panel of Fig. 5 look different since the states of the $3p^53d^{10}4s4p$ configuration are only partly non-autoionizing. The
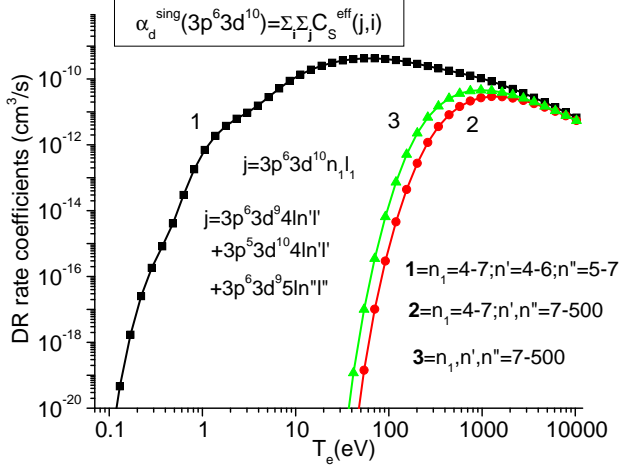
FIG. 7: (Color online) Sum of the contributions from the singly excited $3p^6 3d^{10} nl$ configurations to the total DR rate coefficients $\alpha_d(3p^6 3d^{10})$ as a function of T_e in Cu-like tungsten.
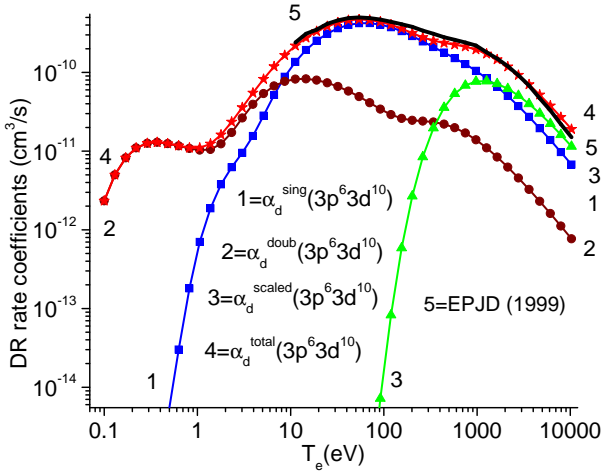

FIG. 8: (Color online) Contributions from the singly excited $3p^6 3d^{10} nl$ and the doubly excited, non-autoionizing $3p^6 3d^9 4l'4l$ and $3p^5 3d^{10} 4l'4l$ levels in Cu-like tungsten to the total DR rate coefficients $\alpha_d(3p^6 3d^{10})$ as a function of T_e. For comparison, the results of Behar *et al.* [51] are presented as well.

largest values of $\alpha_d(3p^6 3d^{10}, j)$ among doubly excited, non-autoionizing states happen for $j = 3p^6 3d^9 4p4f$ when $\alpha_d = 5.98 \times 10^{-11}$ cm^3/s at $T_e = 11$ eV (see curve '5' on the bottom right panel of Fig. 4). That is smaller by a factor of 6.4 than the largest $\alpha_d(3p^6 3d^{10}, j)$ with j for the singly excited $3p^6 3d^{10} 4d$ ^2D term.

V. TOTAL DIELECTRONIC RECOMBINATION RATE COEFFICIENT

The total DR rate coefficients are obtained by summing of the effective emission rate coefficients $C_S^{eff}(j, i)$ (Eq. (2)) over all possible intermediate and final singly and doubly excited states:

$$\alpha_d(i_0) = \sum_i \sum_j C_S^{eff}(j, i). \qquad (5)$$

We have already discussed the contribution from doubly excited states with high-n levels to the DR rate coefficients (sum over i in Eq. (5)). For the total DR rate coefficient one has to consider the contribution from singly excited states and non-autoionizing doubly excited states (sum over j in Eq. (5)). There are about 430 non-autoionizing doubly excited states in the case of Cu-like tungsten. To illustrate the contribution of the $3p^6 3d^9 n'l'nl(L_{12}S_{12})$ LSJ and $3p^5 3d^{10} n'l'nl(L_{12}S_{12})$ LSJ non-autoionizing states to the total DR rate coefficient, we sum those contributions over all angular moments (L_{12}, S_{12}, L, S, J). Finally, we find $\alpha_d(3p^6 3d^{10}, j)$ for the $3p^6 3d^9 n'l'nl$ and $3p^5 3d^9 10n'l'nl$ states.

The sum of the $\alpha_d(3p^6 3d^{10}, j)$ coefficient over j given by doubly exited, non-autionizing levels is shown as curve '1' in Fig. 6. In particular, there are 9 doubly excited, non-autoionizing $3p^6 3d^9 4l'4l$ configurations and 4 doubly excited, non-autoionizing $3p^5 3d^{10} 4l'4l$ configurations. The complete set of the autoionizing configurations includes the $3p^6 3d^9 4f^2$, $3p^5 3d^{10} 4d4l$ ($l = p, d$), $3p^5 3d^{10} 4f4l$ ($l = p, d, f$), $3p^6 3d^9 4l'nl$, $3p^5 3d^{10} 4l'nl$ ($n=5$-6), and $3p^6 3d^9 5l'nl$, ($n=5$-7) configurations.

The contribution from high-n autoionizing levels to the DR rate coefficients involving doubly excited, non-autoionizing configurations is given by curve '2' of Fig. 6. We follow the procedure described in Refs. [27, 28, 30]. In the case of the $3p^6 3d^{10} n'l' - 3p^6 3d^9 n'l'nl$ transitions, we use empirical scaling laws, which can only be implemented to include one-electron $3d-np$, and $3d-nf$ dipole transitions. That means that we consider the following transitions: $3p^6 3d^{10} n'l' - 3p^6 3d^9 n'l'np$ and $3p^6 3d^{10} n'l' - 3p^6 3d^9 n'l'nf$ in the scaling procedure. In the case of the $3p^6 3d^9 n_1l_1 n_2l_2 - 3p^6 3d^9 n_3l_3 n_4l_4$ transitions, we need to consider the $3p^6 3d^9 n_1l_1 n_2l_2 - 3p^6 3d^9 n_1l_1 nl$ transitions in the scaling procedure. In the case of the $3p^6 3d^9 4p^2 - 3p^6 3d^9 n_3l_3 n_4l_4$ transitions, the $3p^6 3d^9 4p^2 - 3p^6 3d^9 4pns$ and $3p^6 3d^9 4p^2 - 3p^6 3d^9 4pnd$ transitions need to be included in the scaling procedure. The final result of the scaling procedure given by curve '2' of Fig. 6 shows a maximum at 970 eV. Even the maximum value of curve '2' is less than any value given by curve '1' of Fig. 6. It should be noted that the ratio of the number of transitions from singly excited $3p^6 3d^{10} nl$ states to autoionizing states to the number of transitions from doubly excited non-autoionizing states to autoionizing states is very small, about 14% only.

TABLE VIII: Total DR rate coefficients α_d^{total} (in cm^3/s) for different temperature values. A[B] means A$\cdot 10^B$.

T_e (eV)	α_d^{total}	T_e (eV)	α_d^{total}
0.10	2.33[-12]	32.12	4.31[-10]
0.13	5.00[-12]	41.75	4.60[-10]
0.17	8.21[-12]	54.28	4.71[-10]
0.22	1.10[-11]	70.56	4.64[-10]
0.29	1.26[-11]	91.73	4.40[-10]
0.37	1.30[-11]	119.25	4.04[-10]
0.48	1.25[-11]	155.03	3.60[-10]
0.63	1.17[-11]	201.54	3.17[-10]
0.82	1.10[-11]	262.00	2.80[-10]
1.06	1.10[-11]	340.60	2.53[-10]
1.38	1.24[-11]	442.78	2.37[-10]
1.79	1.61[-11]	575.61	2.25[-10]
2.33	2.35[-11]	748.30	2.13[-10]
3.03	3.59[-11]	972.78	1.96[-10]
3.94	5.49[-11]	1264.62	1.73[-10]
5.12	8.22[-11]	1644.01	1.46[-10]
6.65	1.19[-10]	2137.21	1.18[-10]
8.65	1.65[-10]	2778.37	9.26[-11]
11.25	2.18[-10]	3611.88	7.03[-11]
14.62	2.76[-10]	4695.44	5.20[-11]
19.00	3.33[-10]	6104.07	3.78[-11]
24.71	3.86[-10]	7935.30	2.70[-11]
		10315.89	1.90[-11]

The sum of the contributions from the singly excited $3p^6 3d^{10} nl$ states to the total DR rate coefficients $\alpha_d(3p^6 3d^{10})$ as a function of T_e in Cu-like tungsten is shown in Fig. 7. Curve '1' displays the $\alpha_d^{\text{sing}}(3p^6 3d^{10}) = \sum_i \sum_j C_S^{eff}(j,i)$ coefficient for $j = 3p^6 3d^{10} nl$ ($n = 4-7$) and $i = 3p^6 3d^9 4f^2$, $3p^5 3d^{10} 4d4l$ ($l = p, d$), $3p^5 3d^{10} 4f4l$ ($l = p, d, f$), $3p^6 3d^9 4l'nl$ (n=5-6), and $3p^6 3d^9 5l'nl$, (n=5-7) configurations of autoionizing states. Curve '2' displays the $\alpha_d^{\text{sing-sc1}}(3p^6 3d^{10}) = \sum_i \sum_j C_S^{eff}(j,i)$ coefficient for $j = 3p^6 3d^{10} nl$ ($n = 4-7$) and $i = 3p^6 3d^9 4l'nl$ (n=7-500), $3p^5 3d^{10} 4l'nl$ (n=7-500), and $3p^6 3d^9 5l'nl$, (n=8-500).

The curve '3' depicts the contributions from singly excited levels with high n, i.e., the $3p^6 3d^{10} nl$ levels with $n > 6$. For these levels, the most important transitions are the $3p^6 3d^{10} nl - 3p^6 3d^9 4pnl$, $3p^6 3d^{10} nl - 3p^6 3d^9 4fnl$, $3p^6 3d^{10} nl - 3p^5 3d^{10} 4snl$, and $3p^6 3d^{10} nl - 3p^5 3d^{10} 4dnl$ transitions. To estimate $Q_d(j,i)$ in Eq. (3) with $j = 3p^6 3d^{10} nl$ and $i = 3p^6 3d^9 4pnl$, $3p^6 3d^9 4fnl$, $3p^5 3d^{10} 4snl$, $3p^5 3d^{10} 4dnl$ $n > 6$, we used the calculated data for $n = 6$ and applied the $1/n^3$ empirical scaling law for the autoionization probabilities A_a and energies E_S. However, the values of A_r for the $3p^6 3d^{10} nl - 3p^6 3d^9 4pnl$, $3p^6 3d^{10} nl - 3p^6 3d^9 4fnl$, $3p^6 3d^{10} nl - 3p^5 3d^{10} 4snl$, and $3p^6 3d^{10} nl - 3p^5 3d^{10} 4dnl$ transitions are almost indepen-

dent of n since this, in fact, is a one-electron transition where the nl electron is a spectator (see, for example, [27, 30, 44]). Again, the calculated data for $n = 7$ and the $1/n^3$ scaling law for A_a are used to estimate the intensity factor $Q_d(j,i)$ in Eq.(3) for the $3p^6 3d^9 5lnl$ autoionization states i with high n. The final value of the $\alpha_d^{\text{sing-sc2}}(3p^6 3d^{10}) = \sum_i \sum_j C_S^{eff}(j,i)$ term for $j = 3p^6 3d^{10} nl$ ($n = 7-500$) and $i = 3p^6 3d^9 4pnl$, $3p^6 3d^9 4fnl$, $3p^5 3d^{10} 4snl$, $3p^5 3d^{10} 4dnl$ ($n = 7-500$) is presented in curve '3' of Fig. 7. It can be seen from this figure that the $\alpha_d^{\text{sing-sc2}}(3p^6 3d^{10})$ values are larger than the $\alpha_d^{\text{sing-sc1}}(3p^6 3d^{10})$ values by a factor of 2-3. The maximum values of the curves '2' and '3' are near 1200 eV and 970 eV, respectively. Curve '1' has a maximum for a smaller temperature, i.e., about 70 eV.

In Fig. 8, we illustrate the results for the total DR rate coefficient $\alpha_d(3p^6 3d^{10})$. The electron temperature varies between 0.1 eV and 10 keV. The resulting curve labeled '4' has a maximum at $T_e \approx 54$ eV and very slowly decreases from a maximum value of 4.71×10^{-10} cm^3/s to 1.90×10^{-11} cm^3/s at 10 keV. Different contributions are shown by curves '1' through '3'. Curve '1' depicts the $\alpha_d^{\text{sing}}(3p^6 3d^{10}) = \sum_i \sum_j C_S^{eff}(j,i)$ coefficient for $j = 3p^6 3d^{10} nl$ ($n = 4-7$) and $i = 3p^6 3d^9 4f^2$, $3p^5 3d^{10} 4d4l$ ($l = p, d$), $3p^5 3d^{10} 4f4l$ ($l = p, d, f$), $3p^6 3d^9 4l'nl$ (n=5-6), $3p^5 3d^{10} 4l'nl$ (n=5-6), and $3p^6 3d^9 5l'nl$, (n=5-7) configurations of autoionizing states. The difference between curve '2' displaying $\alpha_d^{\text{doub}}(3p^6 3d^{10})$ and curve '1' displaying $\alpha_d^{\text{sing}}(3p^6 3d^{10})$ is in the j that includes the $3p^6 3d^9 4l'4l$ and $3p^5 3d^{10} 4l'4l$ doubly excited non-autoionizing states. Curve '3' shows the combined scaled contributions illustrated by curve '2' of Fig. 6 ($\alpha_d^{\text{doub-sc}}(3p^6 3d^{10})$) and curves '2' and '3' of Fig. 7 ($\alpha_d^{\text{sing-sc1}}(3p^6 3d^{10}) + \alpha_d^{\text{sing-sc2}}(3p^6 3d^{10})$).

It is evident from Fig. 8 that the largest contribution to the total DR rate coefficient $\alpha_d(3p^6 3d^{10})$ for low temperature comes from curve '2', while for high temperature the contribution of singly excited state described by curve '1' become dominant. DR rate coefficients presented by Behar *et al.* [51] are shown by curve '5' in Fig. 8. Results in [51] were evaluated in the 10 eV - 10 keV range of temperature. In this interval of temperature our results agree with the results from Ref. [51]. The difference is not more than 20%-30%.

The values of the total rate coefficient α_d^{total} are presented in Table VIII for $T_e = 0.1$ eV to 10.3 keV divided by 45 points on a logarithmic grid $T_e = (0.1 \times 1.3^{N-1})$ eV with $N = 1$–45.

VI. UNCERTAINTY ESTIMATES AND CONCLUSION

In the present paper, we calculated a large set of atomic data needed to describe the dielectronic recombination of Ni-like W^{46+} into Cu-like W^{45+}. Energy levels, wavelengths, weighted radiative transition prob-

abilities, and autoionization rates are calculated for the Cu-like tungsten ion using three theoretical methods, namely, the multiconfiguration relativistic Hebrew University Lawrence Livermore Atomic Code (HULLAC), the Hartree-Fock-relativistic method (Cowan code), and the relativistic many-body perturbation theory method (RMBPT code) for a limited number of states. In order to check the accuracy of those calculations, we performed additional calculations using the second-order and third-order relativistic perturbation theory and relativistic SD all-order method. The SD method, which is a linearized couple-cluster method, includes correlation corrections in a more complete way and is expected to yield more accurate results, especially when correlation corrections are significant. While the SD method includes fourth- and higher-order terms, it omits some third-order terms. These omitted terms are identified and added to our SD data. Also, a comparison is made with all available NIST data.

Our third-order Coulomb correlation energies $(E^{\mathrm{DF}+2+3})$ and the all-order SD energies $E^{\mathrm{DF}+\mathrm{SD}}$ are in excellent agreement (0.002-0.1%) with the recommended NIST data [25]. Such good agreement with available NIST energies allows us to believe that our $E^{\mathrm{DF}+\mathrm{SD}}$ energies for all the $6s\ ^2S_{1/2}$, $6p\ ^2P_J$, and $6d\ ^2D_J$ levels given in Table II can be added to the set of recommended data. We find excellent agreement (0.01%) between our $E^{(\mathrm{DF}+\mathrm{SD})}$ and $E^{(\mathrm{NIST})}$ values for the ionization potential [25], used the difference between our calculated value and experimental value is well within the experimental uncertainty of 0.033%.

The energies calculated by the Cowan code are in a good agreement with the second-order RMBPT energies $(E^{(\mathrm{DF}+2)})$, because a large portion of the correlation contribution is taken into account by the atomic structure code of Cowan [33] through appropriate scaling of the electrostatic integrals. The accuracy of oscillator strengths and transition rates is estimated to be about 20-50% for the largest gf and gA_r values and a factor of 2-5 for the smallest ones. Such large differences are due to substantial contribution from correlation effects. The accuracy of autoionizing rates gA_a are about 20-40% for the largest values of gA_a ($gAa \simeq 10^{13}$-10^{14} s^{-1}).

The calculated atomic data are used to obtain the dielectronic satellite lines as well as the DR rate coefficients. The doubly excited $3p^63d^94f^2$, $3p^53d^{10}4d4l$ ($l = p, d$), $3p^53d^{10}4f4l$ ($l = p, d, f$), $3p^63d^94l'nl$ (n=5-6), $3p^53d^{10}4l'nl$ (n=5-6), and $3p^63d^95l'nl$, (n=5-7) configurations are taken into account to calculate the DR rate coefficients. We find that the contributions of the highly excited states are very important for the calculation of total DR rates. We estimated these contributions using approximate formulae for n up to 100. We calculated the state-selective DR rate coefficients from the ground state of Ni-like W ion to the Cu-like W ion for the singly excited $3p^63d^{10}nl$ (n=4-7), as well as nine $3d$-

core excited, non-autoionizing $3p^63d^94l'4l$ configurations and four $3p$-core excited, non-autoionizing $3p^53d^{10}4l'4l$ configurations. Contributions from the core-excited non-autoionizing states are found to be very important, especially for the low-temperature region, in the determination of the total DR coefficient.

The accuracy of the radiative and nonradiative transition rates and the wavelengths, given in columns "A_a", "gA_r", and "λ" of Tables VI - VII, was discussed in Sect. II. The intensity factor Q_d (Eq. (3)) includes the product $gA_a \times A_r$ and the sum of A_a and A_r. Comparing the results given in columns "A_a" and "$\sum gA_r$", we find that $A_a \gg A_r$. Then, Q_d can be estimated as $Q_d(j,i) \approx g(i)A_r(j,i)$. The accuracy of the radiative transition rates A_r was estimated in the previous section as 20-50% for the largest A_r values and a factor of 2-5 for the smallest one. Therefore, the accuracy of Q_d values should be 20-50% since we list the largest Q_d values in Tables VI - VII. The accuracy of the effective emission rate coefficient $C_S^{\mathrm{eff}} \approx Q_d \times exp(-E_s(i)/kT_e)$ (see the last column of Tables VI - VII) depends on the accuracy of the Q_d and the excitation energies E_S. The E_S values (see the fourth column of Tables VI - VII) are defined as the excitation energy (also called Auger energy) of the autoionizing state relative to the energy of the $3p^63d^{10}$ threshold. We have used the NIST value for the threshold, which has a 0.015% uncertainty (19471,100±2,900) [25]. We believe that the accuracy of the autoionizing state energies is similar to the accuracy of non-autoionizing states given in Table II. Therefore, we can conclude that the effective emission rate coefficients C_S^{eff} are accurate to 25%-55% for most of the cases given in Tables VI - VII.

The total rate coefficient is defined as the sum over the i and j indexes of the effective emission rate coefficients $C_S^{\mathrm{eff}}(i,j)$ (see Eq. (5)). We estimated the accuracy of the effective emission rate coefficients C_S^{eff} to be 25%-55%. This estimate holds for the partial sum up to $i = 7$ and $j =7$. We use scaled values for the sum in Eq. (5) for $i = 8$-100 and $j = 8$-100. The contribution of scaled values in $\alpha_d^{\mathrm{total}}$ is not important for low temperatures T_e = 0.1-200 eV. This contribution increases with increasing T_e; 0.5% for T_e = 200 eV and 52% for T_e = 2140 eV. Therefore, we can conclude that the accuracy of $\alpha_d^{\mathrm{total}}$ is about 25%-55% for the large interval of temperatures (0.1-200)and about a factor of 2 for $T_e > 200$ eV.

[1] T. Pütterich, R. Neu, R. Dux, A. D. Whiteford, M. G. O. Mullane, and the ASDEX Upgrade Team, Plasma Phys. Control. Fusio **50**, 085016 (2008).

[2] R. A. Pitts, A. Kukushkin, A. Loarte, A. Martin, M. Merola, C. E. Kessel, V. Komarov, and M. Shimada, Phys. Scripta **T138**, 014001 (2009).

[3] P. Beiersdorfer, J. Clementson, J. Dunn, M. F. Gu, K. Morris, Y. Podpaly, E. Wang, M. Bitter, R. Feder, K. W. Hill, et al., J. Phys. B **43**, 144008 (2010).

[4] C. S. Harte, C. Suzuki, T. Kato, H. A. Sakaue, D. Kato, K. Sato, N. Tamura, S. Sudo, R. D'Arcy, E. Sokell, et al., J. Phys. B **43**, 205004 (2010).

[5] J. Clementson, P. Beiersdorfer, A. L. Roquemore, C. H. Skinner, D. K. Mansfield, K. Hartzfeld, , and J. K. Lepson, Rev. Sci. Instrum. **81**, 10E326 (2010).

[6] G. F. Matthews, M. Beurskens, S. Brezinsek, M. Groth, E. Joffrin, A. Loving, M. Kear, M.-L. Mayoral, R. Neu, P. Prior, et al., Phys. Scripta **T141**, 014001 (2011).

[7] C. Suzuki, C. S. Harte, D. Kilbane, T. Kato, H. A. Sakaue, I. Murakami, D. Kato, K. Sato, N. Tamura, S. Sudo, et al., J. Phys. B **44**, 175004 (2011).

[8] P. Beiersdorfer, M. J. May, J. H. Scofield, and S. B. Hansn, High Energy Dens. Phys. **8**, 271 (2012).

[9] P. Beiersdorfer, J. K. Lepson, M. B. Schneider, and M. P. Bode, Phys. Rev. A **86**, 012509 (2012).

[10] B. J. MacGowan, S. Maxon, L. B. da Silva, D. J. Fields, C. J. Keane, D. L. Matthews, A. L. Osterheld, J. H. Scofield, G. Shimkaveg, and G. F. Stone, Phys. Rev. Lett. **65**, 420 (1990).

[11] S. R. Elliott, P. Beiersdorfer, B. J. MacGowan, , and J. Nilsen, Phys. Rev. A **52**, 2689 (1995).

[12] M. Klapisch, P. Mandelbaum, A. Bar-Shalom, J. L. Schwob, A. Zigler, and S. Jackel, J. Opt. Soc. Am. **71**, 1276 (1981).

[13] M. Klapisch, J. L. Schwob, B. S. Fraenkel, and J. Oreg, J. Opt. Soc. Am. **67**, 148 (1977).

[14] P. Mandelbaum, M. Klapisch, A. Bar-Shalom, J. L. Schwob, and A. Zigler, Phys. Scr. **27**, 39 (1983).

[15] M. Klapisch, P. Mandelbaum, A. Zigler, C. Bauche-Arnoult, and J. Bauche, Phys. Scr. **34**, 51 (1986).

[16] A. Zigler, M. Klapisch, and P. Mandelbaum, Phys. Lett. A **117**, 31 (1986).

[17] N. Tragin, J.-P. Geindre, P. Monier, J.-C. Gauthier, C. Chenais-Popovics, J.-F. Wyart, and C. Bauche-Arnoult, Phys. Scr. **37**, 72 (1988).

[18] K. B. Fournier, At. Data Nucl. Data Tables **68**, 1 (1998).

[19] G. C. Osborne, A. S. Safronova, V. L. Kantsyrev, U. I. Safronova, P. Beiersdorfer, K. M. Williamson, M. E. Weller, and I. Shrestha, Can. J. Phys. **89**, 599 (2011).

[20] J. Clementson, P. Beiersdorfer, G. V. Brown, and M. F. Gu, Phys. Scr. **81**, 015301 (2010).

[21] Y. Ralchenko, J. Reader, J. M. Pomeroy, J. N. Tan, and J. D. Gillaspy, J. Phys. B **40**, 3861 (2007).

[22] P. Palmeri, P. Quinet, E. Biémont, and E. Träbert, At. Data Nucl. Data Tables **93**, 537 (2007).

[23] A. Kramida, Can. J. Phys. **89**, 551 (2011).

[24] U. I. Safronova, W. R. Johnson, A. Shlyaptseva, and S. Hamasha, Phys. Rev. A **67**, 052507 (2003).

[25] A. E. Kramida and T. Shirai, At. Data and Nucl. Data Tables **95**, 305 (2009).

[26] Ralchenko, Yu., Kramida, A.E., Reader, J., and NIST ASD Team (2011). NIST Atomic Spectra Database (ver. 4.1.0), [Online]. Available: http://physics.nist.gov/asd [2012, April 26]. National Institute of Standards and Technology, Gaithersburg, MD.

[27] U. I. Safronova, A. S. Safronova, and P. Beiersdorfer, J. Phys. B **45**, 085001 (2012).

[28] U. I. Safronova and A. S. Safronova, Phys. Rev. A **85**, 032507 (2012).

[29] S. Schippers, D. Bernhardt, A. Müller, C. Krantz, M. Grieser, R. Repnow, A. Wolf, M. Lestinsky, M. Hahn, O. Novotný, et al., Phys. Rev. A **83**, 012711 (2011).

[30] U. I. Safronova, A. S. Safronova, P. Beiersdorfer, and W. R. Johnson, J. Phys. B **44**, 035005 (2011).

[31] B. W. Li, G. O'Sullivan, Y. B. Fu, and C. Z. Dong, Phys. Rev. A **85**, 052706 (2012).

[32] URL ftp://aphysics.lanl.gov/pub/cowan.

[33] URL http://das101.isan.troitsk.ru/cowan.htm.

[34] A. Bar-Shalom, M. Klapisch, and J. Oreg, J. Quant. Spectr. Radiat. Transfer **71**, 169 (2001).

[35] M. S. Safronova, W. R. Johnson, and A. Derevianko, Phys. Rev. A **60**, 4476 (1999).

[36] U. I. Safronova, I. M. Savukov, M. S. Safronova, and W. R. Johnson, Phys. Rev. A **68**, 062505 (2003).

[37] U. I. Safronova, W. R. Johnson, M. S. Safronova, and J. R. Albritton, Phys. Rev. A **66**, 042506 (2002).

[38] U. I. Safronova, W. R. Johnson, M. S. Safronova, and J. R. Albritton, Phys. Rev. A **66**, 052511 (2002).

[39] A. Derevianko, W. R. Johnson, M. S. Safronova, and J. F. Babb, Phys. Rev. Lett. **82**, 3589 (1999).

[40] W. R. Johnson, U. I. Safronova, A. Derevianko, and M. S. Safronova, Phys. Rev. A **77**, 022510 (2008).

[41] U. I. Safronova and M. S. Safronova, Phys. Rev. A **78**, 052504 (2008).

[42] U. I. Safronova, Phys. Rev. A **82**, 022504 (2010).

[43] M. S. Safronova and U. I. Safronova, Phys. Rev. A **85**, 022504 (2012).

[44] U. I. Safronova, A. S. Safronova, and P. Beiersdorfer, At. Data Nucl. Data Tab. **95**, 751 (2009).

[45] J. Dubau and S. Volonte, Rep. Prog. Phys. **43**, 199 (1980).

[46] U. I. Safronova, R. Bista, R. Bruch, and Yu. Ralchenko, J. Phys. B **42**, 015001 (2009).

[47] U. I. Safronova, A. Safronova, S. Hamasha, and P. Beiersdorfer, At. Data Nucl. Data Tables **92**, 47 (2006).

[48] U. I. Safronova and T. Kato, J. Phys. B **31**, 2501 (1998).

[49] U. I. Safronova, I. Y. Tolstikhina, R. Bruch, T. Tanaka, F. Hao, and D. Schneider, Phys. Scr. **47**, 364 (1993).

[50] U. I. Safronova and A. S. Safronova, Can. J. Phys. **87**, 83 (2009).

[51] E. Behar, P. Mandelbaum, and J. L. Schwob, Eur. Phys. J. D **7**, 157 (1999).